Science of the Total Environment 806 (2022) 150422

Contents lists available at ScienceDirect

Science of the Total Environment

journal homepage: www.elsevier.com/locate/scitotenv

Simulating tree growth response to climate change in structurally diverse oak and beech forests

`Louis de Wergifosse [a,b,*], Frédéric André [a], Hugues Goosse [b], Andrzej Boczon [c], Sébastien Cecchini [d], Albert Ciceu [e,f], Alessio Collalti [g,h], Nathalie Cools [i], Ettore D'Andrea [n], Bruno De Vos [i], Rafiq Hamdi [k], Morten Ingerslev [m], Morten Alban Knudsen [m], Anna Kowalska [c], Stefan Leca [e], Giorgio Matteucci [j], Thomas Nord-Larsen [m], Tanja GM Sanders [o], Andreas Schmitz [o,p,q], Piet Termonia [k,l], Elena Vanguelova [r], Bert Van Schaeybroeck [k], Arne Verstraeten [i], Lars Vesterdal [m], Mathieu Jonard [a]

[a] Earth and Life Institute: Environmental Sciences, UCLouvain, 1, Croix du Sud, 1348 Louvain-la-Neuve, Belgium
[b] Earth and Life Institute: Earth and Climate, UCLouvain, 3, Place Louis Pasteur, 1348 Louvain-la-Neuve, Belgium
[c] Forest Research Institute, Sekocin Stary, ul. Braci Lesnej 3, 05-090 Raszyn, Poland
[d] Office National des Forêts, Département Recherche-Développement-Innovation, Bâtiment B, Boulevard de Constance, 77300 Fontainebleau, France
[e] Forest Management Department, National Institute for Research and Development in Forestry INCDS Marin Drăcea, 128, Bulevardul Eroilor, 077190 Voluntari, Romania
[f] Department of Forest Engineering, Forest Management Planning and Terrestrial Measurements, Faculty of Silviculture and Forest Engineering, "Transilvania" University, 1 Ludwig van Beethoven Str., 500123 Brașov, Romania
[g] Forest Modelling Lab., Institute for Agriculture and Forestry Systems in the Mediterranean, National Research Council of Italy (CNR–ISAFOM), Via Madonna Alta 128, 06128 Perugia, PG, Italy
[h] Department of Innovation in Biological, Agro-food and Forest Systems (DIBAF), University of Tuscia, via San Camillo de Lellis, 01100 Viterbo, VT, Italy
[i] Research Institute for Nature and Forest (INBO), 4, Gaverstraat, 9500 Geraardsbergen, Belgium
[j] Institute for BioEconomy, National Research Council of Italy (CNR–IBE), via Madonna del Piano, 10 50019 Sesto Fiorentino, FI, Italy
[k] Royal Meteorological Institute of Belgium, 3, Avenue circulaire, 1180 Brussels, Belgium
[l] Department of Physics and Astronomy, Ghent University, 86, Proeftuinstraat, 9000 Ghent, Belgium
[m] Department of Geosciences and Natural Resource Management, University of Copenhagen, Rolighedsvej 23, DK-1958 Frederiksberg C, Denmark
[n] Institute for Agriculture and Forestry Systems in the Mediterranean, National Research Council of Italy 8 (CNR–ISAFOM), P. le Enrico Fermi 1 Loc. Porto del Granatello, 80055 Portici, NA, Italy
[o] Thünen Institute of Forest Ecosystems, Alfred-Moeller-Str. 1, Haus 41/42, 16225 Eberswalde, Germany
[p] State Agency for Nature, Environment and Consumer Protection of North Rhine-Westphalia, 10, Leibnizstraße, 45659 Recklinghausen, Germany
[q] Department of Silviculture and Forest Ecology of the Temperate Zones, University of Göttingen, 1, Büsgenweg, 37077 Göttingen, Germany
[r] Centre of Ecosystem, Society and Biosecurity, Forest Research, Alice Holt Lodge, Farnham, Surrey GU10 4LH, UK

HIGHLIGHTS

- Uneven-aged mixed forests are advocated to reinforce resilience under global change.
- Simulating their response to climate change requires process-based tree level models.
- The HETEROFOR model was successfully evaluated on many European monitoring sites.
- Stand properties explain the major part of the inter-site productivity variability.
- Forest response to climate change mainly depends on initial climate conditions.

GRAPHICAL ABSTRACT

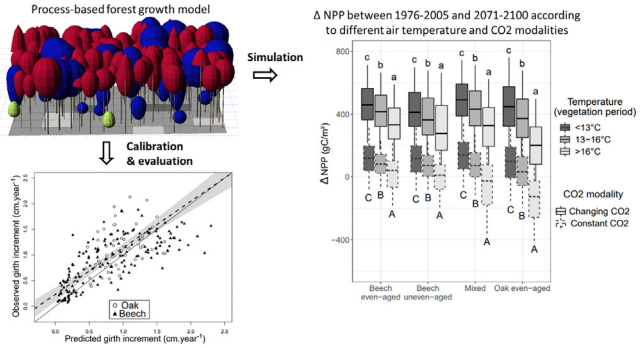

* Corresponding author at: Avenue Jules Malou 65, Etterbeek 1040, Belgium.
E-mail address: dewergifosse.louis@gmail.com (`L. de Wergifosse).

https://doi.org/10.1016/j.scitotenv.2021.150422

ARTICLE INFO

Article history:
Received 8 June 2021
Received in revised form 23 August 2021
Accepted 14 September 2021
Available online 20 September 2021

Editor: Elena PAOLETTI

Keywords:
Temperate broadleaved forest
Process-based modelling
Productivity projections
Climate change
Site effect
HETEROFOR

ABSTRACT

This study aimed to simulate oak and beech forest growth under various scenarios of climate change and to evaluate how the forest response depends on site properties and particularly on stand characteristics using the individual process-based model HETEROFOR. First, this model was evaluated on a wide range of site conditions. We used data from 36 long-term forest monitoring plots to initialize, calibrate, and evaluate HETEROFOR. This evaluation showed that HETEROFOR predicts individual tree radial growth and height increment reasonably well under different growing conditions when evaluated on independent sites.
In our simulations under constant CO_2 concentration ($[CO_2]_{cst}$) for the 2071-2100 period, climate change induced a moderate net primary production (NPP) gain in continental and mountainous zones and no change in the oceanic zone. The NPP changes were negatively affected by air temperature during the vegetation period and by the annual rainfall decrease. To a lower extent, they were influenced by soil extractable water reserve and stand characteristics. These NPP changes were positively affected by longer vegetation periods and negatively by drought for beech and larger autotrophic respiration costs for oak. For both species, the NPP gain was much larger with rising CO_2 concentration ($[CO_2]_{var}$) mainly due to the CO_2 fertilisation effect. Even if the species composition and structure had a limited influence on the forest response to climate change, they explained a large part of the NPP variability (44% and 34% for $[CO_2]_{cst}$ and $[CO_2]_{var}$, respectively) compared to the climate change scenario (5% and 29%) and the inter-annual climate variability (20% and 16%). This gives the forester the possibility to act on the productivity of broadleaved forests and prepare them for possible adverse effects of climate change by reinforcing their resilience.

1. Introduction

In the future, European temperate forests will experience warmer conditions, the magnitude of which will depend on the climate zone and on the greenhouse gas emission pathway (Coppola et al., 2020; Jacob et al., 2014). Changes in rainfall regime are also expected with generally wetter winters, especially in the North of Europe but drier summers in the South (Spinoni et al., 2020; Coppola et al., 2020). Finally, heat waves, droughts and storms are likely to become more frequent and severe compared to the current observed climate (for more details, see Sillmann et al., 2013; Spinoni et al., 2020).

The combined effects of changes in atmospheric CO_2 concentration, air temperature, and rainfall will affect the growth of temperate broadleaved forests but the effects are expected to differ depending on whether the sites are located at the warm, cold or dry margin of their species distribution range (Jump et al., 2006; Dulamsuren et al., 2017). Additionally, stand characteristics and soil properties as well as atmospheric deposition will modulate the climate change effect, which complicates the forest dynamics projections (Anderegg et al., 2018; Martin-Benito and Pederson, 2015)

Future response of European forests to climate change can be predicted using different modelling approaches, which are designed to answer specific questions at different spatial and temporal scales and using different initialisation data (Ruiz-Benito et al., 2020; Reyer et al., 2020). Dynamic global vegetation models (DGVM) and forest landscape models (FLMs) provide information on continental or global estimates of carbon exchange or on how climate change affects long-term forest dynamics but have a simplified eco-physiological process description and coarse stand-level spatial representation due to their large-scale and long-term perspective (Reyer, 2015; Maréchaux et al., 2021).

To account for local environmental conditions (soil, climate, tree species) more in-depth, process-based stand and cohort models were designed but they generally do not consider the within-stand heterogeneity and the tree-tree interactions (e.g. big leaf or average tree approaches; e.g. Collalti et al., 2016). Therefore, they display good predictive ability for even-aged monocultures but the oversimplified spatial representation of the stand structure can be problematic for studies in more complex stands (e.g. Simioni et al., 2016; Morin et al., 2021). To fully account for the spatial heterogeneity in structurally-complex stands, spatially explicit individual-based models (IBMs) are required (Pretzsch et al., 2015). Given the data required for their initialisation, very few spatially explicit IBMs were used to estimate the impact of future climate changes on forest growth for more than a couple of sites (see for example the models VS-Lite in Tolwinski-Ward et al., 2013 or VS-model in Anchukaitis et al., 2006).

The HETEROFOR model has been specifically designed to simulate individual tree growth in structurally complex stands based on a resource-sharing approach and to test the ability of innovative silvicultural systems to improve forest resilience to climate change (de Wergifosse et al., 2020a; Jonard et al., 2020). So far, it has been calibrated and used to simulate the impact of climate change on a couple of forests in Southern Belgium (de Wergifosse et al., 2020b). Yet, one can assume that calibrating a process-based model on a large range of ecological conditions will increase its generality and robustness (e.g. Forrester et al., 2021a), particularly for simulations under changing climatic conditions. Hence, in this study we aimed to evaluate the HETEROFOR model on contrasting site conditions benefiting from harmonised data collected in long-term monitoring networks (ICP Forests level II plots and LTER sites). The calibrated and validated model was subsequently used to respond to the following questions:

(i) How climate change will affect oak and beech tree growth in European temperate forests?

We hypothesized that CO_2 fertilisation will have a dominant effect but that the negative effects of the increased water stress and respiration costs will be compensated by a longer vegetation period under the hypothesis of a constant atmospheric CO_2.

(ii) What will be the relative importance of the long-term climate change effects on tree growth compared to the inter-site and inter-annual variability?

We considered that climate change effect will be larger than the inter-annual climate variability.

(iii) How the forest response to climate will be modulated by the local soil, stand and climate conditions?

We hypothesized that the climate change will be more detrimental in even-aged beech stands than in uneven-aged, mixed or oak dominated stands, in sites with a low soil water reserve and/or under warm and dry climates.

These questions were treated by simulating the response of temperate oaks and European beech to climate change for a set of European sites covering a large range of environmental conditions (soil and climate) and stand characteristics. The inter-site variability was decomposed in its components (stand, soil and climate) to evaluate how they affect the response of tree growth to climate change.

2. Material and methods

2.1. Site description

For the model evaluation, 36 forest monitoring plots distributed over Europe (for measurement periods between 5 and 25 years) and covering a large range of ecological conditions were selected. The plot size ranges from 0.2 to 1.8 ha. 30 of the plots are part of the level II monitoring network of ICP Forests (Ferretti and Fischer, 2013). The six remaining plots are located in Baileux (Belgium) and in Cansiglio (Italy). The three plots in Baileux were installed to study the impact of species mixture on forest ecosystem functioning. In Cansiglio, the three plots are part of the project LIFE CLIMARK (LIFE16 CCM/ES/000065) which promote sustainable forest management as a tool to face climate change.

All these plots were selected based on their species composition (broadleaved forests dominated by either temperate oak or European beech) and the data availability (for the model initialisation) while seeking to maximize the diversity of stand types, soils and climates (Tables A.1 and A.2). In the study, sessile and pedunculate oaks are not differentiated and will be called "oak" while European beech will be referred to as "beech" in the following.

The 36 plots of the study are distributed into 32 sites with 10 in the continental, three in the mountainous and 19 in the oceanic temperate zones (see FAO, 2012 for climate zone definition). The climates covered by the study sites are representative of those encountered in the distribution range of oak and beech (Sykes et al., 1996; Kölling, 2007), with mean annual temperature (MAT) ranging from 4.8 to 12.9 °C and mean annual precipitation (MAP) from 612 to 2153 mm (Table A.1) for the period 1976-2005.

The stands were classified according to their composition and structure. We considered a stand as pure when the main species represented at least 75% of the total basal area. The same threshold was used to distinguish even-aged from uneven-aged stands. A stand was considered even-aged when 75% of trees (in basal area) were in the same cohort. The cohorts were defined by analysing the tree distributions by size class. Among the 36 stands, 10 were classified as even-aged oak-dominated, 13 as even-aged beech-dominated, 3 as uneven-aged beech-dominated and 10 as uneven-aged oak and beech mixtures. In addition to the variability in species composition and stand structure, the stands were also very diverse in terms of mean trunk girth (42.4 to 176.6 cm), dominant height (16.9 to 36.8 m) and basal area (13.6 to 53.9 m^2 ha^{-1}) (Table A.2).

Among the 12 classes of the soil textural triangle elaborated by the United States Department of Agriculture (Soil Science Division Staff, 2017), 9 were represented in the study sites. This variability in soil texture explains some of the large range in maximum extractable water (MEW: 154 to 594 mm) which is also due to variations in the coarse fraction (0 to 41%) and soil depths (1 to 1.6 m) (Table A.1). Detailed information for MEW calculation is provided in Eq. (80) of de Wergifosse et al. (2020a).

2.2. Modelling approach

2.2.1. Model description

For the simulations, we used the spatially explicit, individual- and process-based model HETEROFOR that has been implemented in the CAPSIS simulator (Dufour-Kowalski et al., 2012) and is especially convenient for simulating the impact of climate change on structurally complex stands. In the following, we present a brief overview of the model functioning while we refer to Jonard et al. (2020) and de Wergifosse et al. (2020a) for a more in-depth description.

The model determines the key phenological phases of the deciduous species (budburst, leaf yellowing and falling) from meteorological data. Then, the radiation intercepted by each tree is calculated with the SAMSARALIGHT library using a ray-tracing approach (Courbaud et al., 2003; André et al., in press). From the radiation intercepted by the foliage and the soil water potential (calculated with the water balance routine), the gross primary production (GPP, in kgC $tree^{-1}$ h^{-1}) of each tree is estimated hourly with the biochemical photosynthesis model of the CASTANEA library (Dufrêne et al., 2005). The net primary production (NPP, in kgC $tree^{-1}$ h^{-1}) is obtained empirically from the GPP through the Carbon Use Efficiency (CUE = NPP / GPP) approach. CUE varies with tree size and shape, competition for light and MAT. NPP is first allocated to foliage and fine roots (<2 mm) by ensuring a functional balance and then to structural components using allometric equations, which allows deriving tree dimensional growth. The water balance routine partitions rainfall into throughfall, stemflow and interception (André et al., 2008), calculates tree transpiration and evaporation from foliage, bark and soil using the Penman- Monteith equation (Monteith, 1965) and estimates root water uptake (Couvreur et al., 2012) and soil water movements based on the Darcy law.

In the model version 1.0 (see Jonard et al., 2020; de Wergifosse et al., 2020a), water balance was calculated before photosynthesis, and the stomatal conductance for water did not depend on atmospheric CO_2 concentration. In the model version used here, the two processes were more closely coupled and the stomatal conductance was calculated in the same way for water and CO_2 using the formulation of Ball et al. (1987) adapted to the tree level by accounting for the influence of tree height (Schäfer et al., 2000). Compared to version 1.0, this modification and the changes in the phenology module and CUE function described hereafter are the only model updates.

2.2.2. Model parameterisation

The HETEROFOR model requires parameters most of which are species-specific. The parameters used for oak and beech in this study are valid at the European scale for a large range of ecological conditions and provided in supplementary materials (Table A.3). Some species parameters (e.g. specific leaf area, leaf size, leaf/needle turnover, leaf retranslocation, taper function, volume functions, drought sensitivity) were obtained directly from the literature on functional traits, tree ecophysiology or dendrometry. The parameters used for carbon allocation were obtained by fitting allometric relationships, for example, leaf biomass or aboveground woody biomass from trunk diameter at breast height (dbh) and/or tree height. To make these adjustments, we benefited from biomass data gathered for meta-analyses (see details in Table A.3). Other parameters were associated with relationships predicting some tree dimensions (crown base height and crown radius) based on dbh and/or height. These relationships were fitted using the tree measurement data collected at the various study sites.

Budburst parameters for oak and beech were taken from Duputié et al. (2015), who use phenological models close to those implemented in HETEROFOR (the optimum model for oak and the sigmoid model for beech). Only the optimum response function during chilling (Eq. (1) in de Wergifosse et al., 2020a, 2020b) was different and had to be adapted to correspond to that given in Duputié et al. (2015) (itself based on Wang and Engel, 1998). Leaf yellowing and fall parameters were empirically fitted with the observations provided for 13 of the study sites located in Belgium, Germany, France and Romania.

Most parameters were derived directly from measurements or by fitting relationships. However, two very important aspects required to run the model for their calibration: (i) the CUE, and (ii) the tree height growth function.

We used an empirical relationship to estimate individual CUE from dbh (cm), total tree height (h in m), crown diameter (D in m), height of crown base (hcb in m), light competition index (LCI: the ratio between the absorbed radiation calculated with and without neighbouring trees), and MAT (in °C). These variables were selected to account for the effects of the tree size and shape, the local light competition and MAT on the CUE (Piao et al., 2010; Collalti and Prentice, 2019). The CUE concept allows converting the GPP into NPP and therefore implicitly accounts for the growth and maintenance respiration. While the growth respiration (i.e. the metabolic cost of building new tissues) is

proportional to NPP, the maintenance respiration depends on temperature and on the living biomass whose proportion changes with tree size and shape, and competition conditions (Collalti et al., 2020). The living biomass proportion is higher in trees experiencing limited competition with well-developed crown. Indeed, such trees have a higher proportion of branches, leaves and fine roots and produce larger growth rings that increase their sapwood proportion (Canham et al., 2004).

$$CUE = \alpha + \beta\, dbh_{cm} + \gamma\, {dbh_{cm}}^2 + \delta\, h + \varepsilon\, h^2 + \zeta\, \frac{h}{dbh_m} + \eta\, Dd_{index} + \theta\, \frac{h-hcb}{h} + \iota\, ln\,(LCI) + \kappa\, MAT + error \quad (1)$$

with dbh and h characterizing the tree size; h/dbh_m, Dd_{index} (standardized crown to stem diameter ratio see Section 2.2.3 in Jonard et al., 2020) and $\frac{h-hcb}{h}$ describing the tree shape independently of its size (slenderness, crown horizontal and vertical extension); LCI, the light competition index varying between 0 (no light reaching the tree) and 1 (no competition); MAT, the mean annual air temperature; α to κ, fitting parameters.

Eq. (1) was fitted with CUE data obtained by dividing the reconstructed NPP (see Section 2.2.7 in Jonard et al., 2020) by the predicted GPP. The principle of parsimony was applied, and non-significant effects were removed using a stepwise forward procedure based on BIC (Bayesian information criterion).

The height growth function estimates the annual height growth (m yr^{-1}) based on the light competition index (LCI), the potential height growth (Δh_{pot} in m yr^{-1}), the height (in m), and/or the dbh (in cm) considering also an error term (standard error of the residuals).

$$\Delta h = \alpha + \beta\, LCI + \gamma \Delta h_{pot} + \delta {\Delta h_{pot}}^2 + \varepsilon\, h + \zeta\, h^2 + \eta\, dbh + error \quad (2)$$

with $\Delta h_{pot} = \frac{\Delta dbh^2 h}{\frac{dbh^2}{100}}$

Δh_{pot} is the potential height increment if all the growth potential is allocated to the primary growth in height (and nothing is left for the secondary growth in dbh). Then, variables describing the tree size (dbh, h) and the local light competition (LCI) are used to determined how this growth potential is distributed between primary and secondary growth. Height growth rate is known to first increase with tree size and then decrease (Koch et al., 2004; Briseño-Reyes et al., 2020). By considering the effect of the local light competition, Eq. (2) accounts for the fact that trees undergoing stronger light competition invest more carbon for height growth to minimize overtopping by neighbours and maximize light interception (Jucker et al., 2015; Trouvé et al., 2015). Eq. (2) was fitted based on tree growth data and on the mean LCI estimated by HETEROFOR for the period during which height growth was monitored. For the CUE and the height growth functions, the parameter values are given in Table A.3 for oak and beech.

2.2.3. Model initialisation

During the initialisation phase, the model requires various data describing: (i) the soil horizons, (ii) the stand and (iii) the meteorological conditions at an hourly time step (see below for description). The data necessary for the model initialisation were collected from the national focal centres regarding the ICP Forests level II plots and from the site managers for the Baileux (LTER site, Belgium) and Cansiglio (Italy) experimental sites, which measurement periods range from 5 to 25 years.

2.2.3.1. Soil data. For each soil horizon, the soil input data include: thickness, volumetric coarse fraction, bulk density, sand, silt and clay contents, organic carbon content and fine root proportion. The maximum soil depth was fixed to 1.6 m for the sake of comparability among sites. When the soil depth was less than 1.6 m, the real soil depth was retained.

2.2.3.2. Stand data. The stand inventory data describe site and tree level characteristics. Among the site level information, the plot geographic coordinates, slope and orientation are required to simulate the radiation transfer with the ray tracing approach. Tree position and dimensions (diameter at breast height: dbh; tree height, height to crown base, height of largest crown extension, crown radii in the four cardinal directions) are necessary input variables for the simulations. However, only dbh is really essential as the other tree dimensions can be estimated based on empirical relationships during a pre-processing phase. Depending on the data availability for each tree species, the age-dependent relationships used for the gap filling were either common for various sites or site-specific. For each tree dimension and each site, the parameters of the equations used to estimate them are provided in de Wergifosse (2021). Finally, tree positions are required to run the model. Missing coordinates were randomly generated by ensuring that two trees were not placed too close from each other according to their crown dimensions.

2.2.3.3. Meteorological data. Meteorological variables needed by HETEROFOR include air temperature, rainfall, incoming short-wave solar radiation, relative humidity, and wind speed at an hourly resolution. As far as possible, we selected sites for which these variables were monitored in open field stations in close proximity to the forest stand. In order to have continuous time series covering the period of the tree growth monitoring, we used ERA5 reanalysis data (Hersbach et al., 2020) corrected based on meteorological observations. The biases in the ERA5 data (when compared to meteorological observations) were corrected using the quantile mapping method from the R package downscaleR (Bedia et al., 2020), which allowed us to obtain continuous hourly data from 1979 to 2019. For some sites, we had only daily meteorological observations. In this case, bias correction was applied at the daily time step and then, the daily cycle of ERA5 was added to obtain hourly values.

2.2.4. Model performances

The model evaluation is focused on tree dimensional growth and phenology. For tree growth, we tested the ability of the model to reproduce the individual increment in tree height an girth estimated on 5 to 10-year periods (n = 10,108 trees in 36 stands). The tree growth evaluation was conducted by considering each tree separately or grouped in 10 cm girth classes in each plot. In a second time and to evaluate the robustness of our model, the CUE function was recalibrated on half of the sites (calibration dataset, n = 4859 trees in 18 stands) and an independent evaluation was carried out on the remaining sites (evaluation dataset, n = 5249 trees in 18 stands). The partitioning of the sites between the calibration and evaluation datasets was achieved in order to cover the diversity of stands, soils, and climates in both sets.

Budburst, leaf yellowing and fall were observed only on a limited number of sites (13). The dates characterizing these phenological phases were those for which they were completed for 50% of the trees. For the budburst, the comparison of the observed and predicted dates provided an independent evaluation while it gave only an indication of the calibration quality for the leaf yellowing and fall since the same observations were used to adjust some parameters (the leaf yellowing parameter, y and the falling rate, R_{fall}; see Table A.3).

Multiple statistical indices were used to test the model predictive ability. First, we calculated the bias (average error, AE) or the relative bias (normalized average error, NAE). The NAE is the difference between the average values of the predictions and observations (i.e. AE), divided by the average of observations. Bias significance was assessed using a paired t-test. To check the absence of bias throughout the range of values (and not only on the average), regression tests were done using the Deming fitting procedure (mcr package in R) since both observations and predictions were characterised by uncertainties. The error ratio was determined based on the variances of observations and predictions. Finally, we estimated the agreement between

observations and predictions based on the Pearson's correlation (r) and on the root mean square error (RMSE), which provides information on the prediction accuracy. All the tests were carried out with R software (R core Team, 2020).

2.3. Simulation experiment

2.3.1. Simulation set-up

The set of 36 plots available for this study is limited compared to the diversity of conditions in Europe's forests. Furthermore, the effects of the site components (soil, stand and climate) can be confounded. To disentangle the various components of the site effect and to assess how they impact the tree growth response to climate change, we ran the simulations for a large number of 'virtual' plots, representing combinations of the different soils, stands and climates from the 36 plots. As a full factorial experiment was not feasible given the number of possible combinations (36 soils × 36 stands × 32 climates = 41,472), we selected subsets of stands, soils and climates representative of the diversity of oak and beech growth conditions in Europe. Twelve stands were chosen, three in each of the four stand categories (even-aged beech/oak, uneven-aged beech/mixed); six soils, three in each of the two soil types (low and high MEW), and nine climates, three in each of the three climate zones (continental, mountainous and oceanic). Nine virtual sites were created for each of the 24 combinations of site component categories (9 replicates × 4 stand types × 2 soil types × 3 climate zones = 216 virtual sites).

Two consecutive 15-year simulations were conducted for the historical period (1976-1990, 1991-2005) and for the future (2071-2085, 2086-2100). For the latter, two RCP (Radiative Concentration Pathway) scenarios (Meinshausen et al., 2011; Van Vuuren et al., 2011) were used: RCP4.5 and RCP8.5. The scenario names depict the increase in radiative forcing in 2100 relative to preindustrial levels (+ 4.5 W m $^{-2}$, + 8.5 W m $^{-2}$). A 15-year period was retained as it corresponds to the average monitoring period for which we know the cutting operations. For a given period, the stand conditions were therefore reinitialized after 15 years to avoid that stand characteristics differ too much with time among RCP scenarios. Indeed, in this case, the direct climate change impact could be partly confounded with an indirect effect due to a divergence in stand evolution. For these 15-year periods, we started with the stand conditions observed at the beginning of the monitoring period and we applied the same thinning operations (or mortality rates) as those observed during the monitoring period in the stand selected for the creation of the virtual sites.

One of the main uncertainties when simulating long-term forest growth is whether or not the CO_2 fertilisation effect can persist (Terrer et al., 2019; Wang et al., 2020). In order to highlight this effect, the simulations were run with a constant atmospheric CO_2 concentration ($[CO_2]_{cst}$ = 380 μmol mol^{-1}) or a CO_2 concentration changing over time ($[CO_2]_{var}$) according to the corresponding RCP scenario.

2.3.2. Climate projections

In order to account for the large uncertainty in climate projections associated with the various global and regional climate models (Kjellström et al., 2018; Christensen and Kjellström, 2020), we used climate projections produced by two different regional climate models (RCM) within the European branch of the Coordinated Regional Downscaling Experiment (EURO-CORDEX; Giorgi et al., 2009; Jacob et al., 2020): ALARO-0 (Giot et al., 2016) and RCA4 (Samuelsson et al., 2011). Three-hourly time series with a spatial resolution of 12.5 km were used. These RCMs were driven at their boundaries by the results of two different global climate models (GCM): CNRM-CM5 (Voldoire et al., 2013) for ALARO-0 and IPSL-CM5A (Dufresne et al., 2013) for RCA4. In the following, these combinations of GCM and RCM will be called CNRM-ALARO and IPSL-RCA4. Climate projections can still substantially differ from *in situ* measurements due to model biases and representativity errors. They were therefore bias-corrected using the quantile mapping method and discretized (conversion from three to one-hour time step).

2.3.3. Model simulation analysis

The impact of climate change on NPP and the other tree growth-related variables (vegetation period length and transpiration deficit) was assessed separately for the different categories of stand, soil and climate and for the two CO_2 modalities (constant and changing over time). The stand net primary production simply consists of the sum of individual tree NPP scaled per square meter per year. We define the vegetation period length as the number of days between the time the green leaf proportion reaches 50% during spring and when it drops below 50% during fall. The transpiration deficit (mm) is the difference between the potential transpiration (estimated by considering no soil water limitation on the stomatal conductance) and the actual transpiration (taking the soil water limitation into account). Transpiration deficit was calculated for all trees annually and was then aggregated at the stand scale and divided by the stand area.

To investigate whether the climate scenarios generated significant differences in the response variables, an unpaired Mann-Whitney test was conducted between the historical period and the future projections, whereas a paired Wilcoxon signed-rank test was performed between the two RCP scenarios as they correspond to the same period (Wilcoxon, 1945). We chose those non-parametric tests due to their lower sensitivity to non-normal variables than parametric tests. Those tests were produced in R using the lme4 package (Bates et al., 2014).

To evaluate the relative importance of climate change effects on tree growth compared to the spatial (stand, soil and climate) and temporal variability, we used a linear mixed model, which considers the climate scenario (considering both the RCP scenario and the differences between the climate models) as a fixed effect and stand, soil and climate as random factors. In addition, the interactions between the three site components (soil, stand, and climate) and the climate scenario were also included in the model as random coefficients to account for the impact of the site components on the climate change effect as follows:

$$NPP \sim [scenario]_{fixed} + [stand + soil + climate + (stand + soil + climate).scenario]_{random} \quad (3)$$

We considered the stand, soil and climate as random factors because there are many stands, soils and climates but we are not interested in their effects for a particular stand, soil or climate. Instead, we want to account for their effects in the correlation structure of the dataset and to evaluate their contribution in the total NPP variability while limiting the number of parameters in the model.

The residual distribution normality of the models was checked with a Kolmogorov-Smirnov test. The partial R^2 of the fixed effect in the model was considered as the difference between the R^2 of the model when the effect was included (but without the interactions) and without the considered effect. The partial R^2 of the random effects was calculated as the ratio of the variance component for the effect to the total variance.

To identify the underlying factors at the origin of the stand, soil and climate effects on NPP change in response to climate change, multivariate linear models were elaborated by selecting the main explanatory variables using a stepwise forward procedure based on BIC (Bayesian information criterion). The change in NPP was estimated between the mean NP*P* value during the historical period and the annual NPP during 2071-2100 under the RCP8.5 scenario. A set of integrative variables describing the stand, soil and climate characteristics were considered as potential predictors: the beech and oak basal area proportion (%), the stem number per ha (N ha^{-1}), the basal area (m^2 ha^{-1}), the mean dbh and its standard deviation, and the dominant height (height of 100 tallest trees per ha; in m). Concerning soil, the soil depth, MEW and the mean granulometry (sand, silt and clay contents) were chosen.

Finally, the climate-related variables selected were the mean temperature (°C) and total precipitation (mm), both annually and for the vegetation period (May to September) and the atmospheric CO_2 concentration. They were averaged over the historical period and their change for the two RCP scenarios was also considered. All the statistical analyses were carried out with R software (R core Team, 2020) except the linear mixed models, which were fitted with the JMP software (JMP®).

3. Results

3.1. Model performances

3.1.1. Tree growth

The model was evaluated on tree height growth and radial increment for each of the three datasets (i.e. the whole data, calibration and evaluation data). For the whole dataset, the prediction biases were limited for both height and radial growth. The identity line was always comprised within the confidence interval of the regression of observations vs predictions (Fig. 1). The prediction precision was however much higher for girth than for height growth. Girth increment was better predicted for beech than for oak while the opposite was found for height increment, especially when considering RMSE and Pearson's r. Compared to the prediction quality obtained using the calibration dataset, model performances were only slightly deteriorated with the evaluation dataset, except for beech height growth (Table 1).

3.1.2. Phenology

The prediction of the budburst date suffered from a bias of only –0.4 day for beech and 2.8 days for oak, both statistically non-significant and the Pearson's r amounted to 0.81 and 0.88, respectively. Apart from a little delay in the prediction of oak budburst for the sites with an early leafing, the budburst was well reproduced for both tree

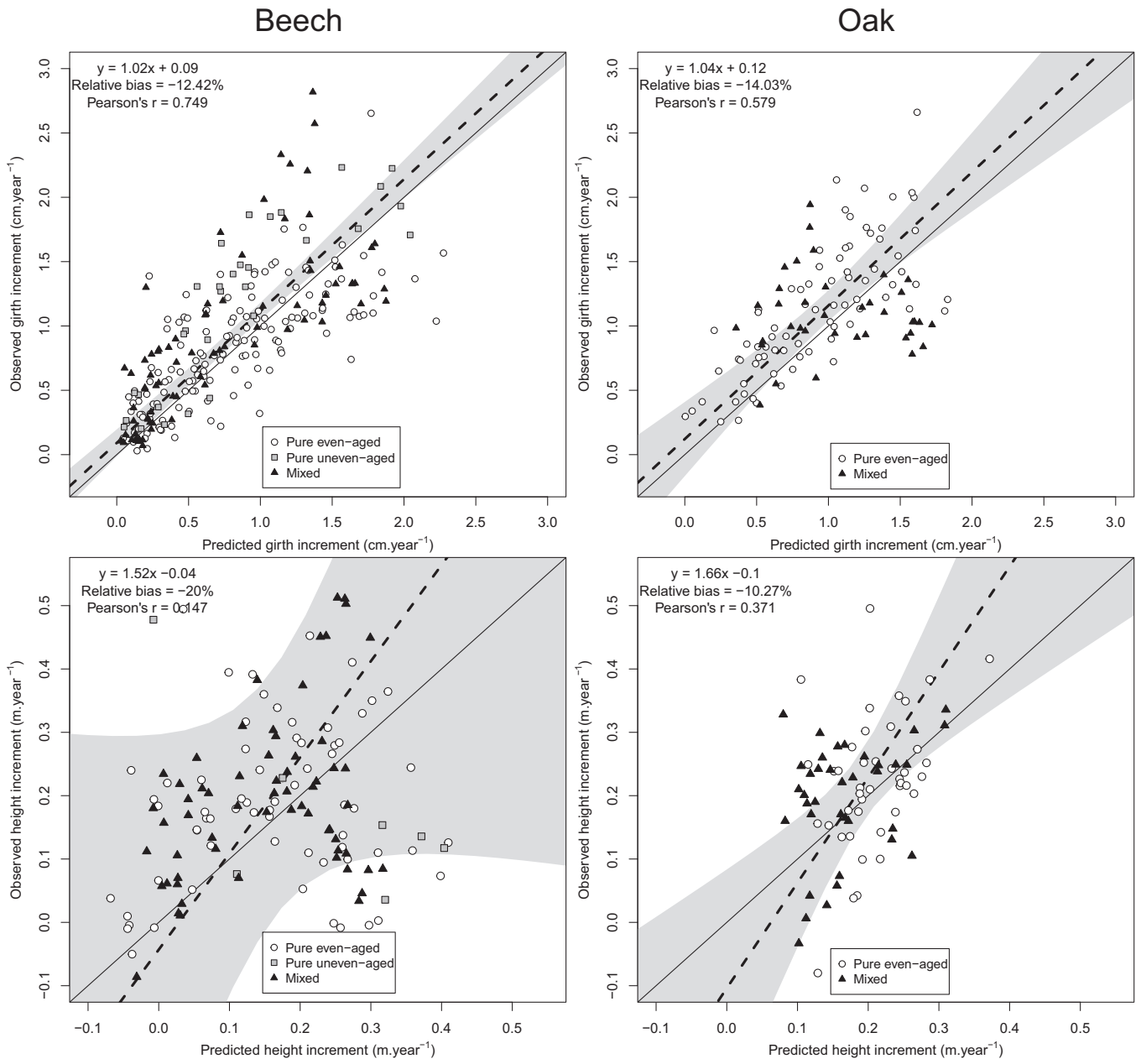

Fig. 1. Comparison of the observed and predicted girth (top) and height (bottom) increments aggregated by 10 cm girth classes for beech (left) and oak (right). Using the whole dataset, the prediction quality is assessed based on the relative bias, the Pearson's r and the Deming regression test (position of the identity line (solid line) with respect to the confidence interval of the regression line (dashed line)).

Table 1
Statistical evaluation of the predicted height and girth increments (vs. individual observations) over 5 to 10-year periods for the entire, calibration and evaluation datasets using normalized average error (NAE), paired *t*-test, Deming regression parameters, root mean square error (RMSE) and Pearson's correlation (Pearson's r). Standard deviation or confidence intervals are provided in parentheses.

Tree species	NAE	Paired *t*-test	Deming regression		RMSE	Pearson's r
CUE calculation		*P* value	intercept	slope		
Height increment (m yr^{-1})						
OAK						
All data	−0.10	0.053	−0.10 (±0.19)	1.66 (±0.95)	0.10	0.371
Calibration data	0.04	0.717	−0.27 (±0.56)	2.33 (±2.81)	0.11	0.286
Evaluation data	−0.20	0.001	−0.01 (±0.21)	1.32 (±1.10)	0.09	0.340
BEECH						
All data	−0.20	0.022	−0.04 (±0.34)	1.52 (±1.74)	0.20	0.147
Calibration data	−0.30	0.000	0.01 (±0.11)	1.33 (±0.58)	0.16	0.530
Evaluation data	−0.07	0.546	0.50 (±0.58)	−1.68 (±2.77)	0.22	−0.132
Girth increment (cm yr^{-1})						
OAK						
All data	−0.14	0.000	0.12 (±0.29)	1.04 (±0.27)	0.44	0.579
Calibration data	−0.13	0.008	0.16 (±0.37)	0.99 (±0.34)	0.46	0.599
Evaluation data	−0.14	0.004	−0.11 (±0.70)	1.28 (±0.69)	0.42	0.463
BEECH						
All data	−0.12	0.004	0.09 (±0.11)	1.02 (±0.11)	0.41	0.749
Calibration data	−0.16	0.000	−0.04 (±0.17)	1.25 (±0.19)	0.41	0.803
Evaluation data	−0.09	0.013	0.20 (±0.12)	0.86 (±0.12)	0.39	0.747

species. Leaf yellowing and leaf fall were predicted with less precision than the budburst (lower Pearson's r) but again without significant bias. Moreover, the identity line was within the confidence interval of the regression of observations vs predictions (Fig. 2).

3.2. Simulations on virtual sites

3.2.1. Vegetation period

Since phenology was not CO_2 dependent in the model, no distinction was made between the two CO_2 modalities. In addition, the simulations for the two types of climate projections were treated together. Compared to the historical period, the vegetation period increased with the intensity of the radiative forcing for both tree species (Fig. 3). For beech, the vegetation period increase was more pronounced under the mountainous climate (+3.9 days per decade for RCP8.5) and then in the continental and oceanic zones (+3.5 and +2.9 days per decade for RCP8.5, respectively). For oak, the vegetation period extension was greater than for beech. It was similar under continental and mountainous climates (+4.3 and +4.4 days per decade for RCP8.5, respectively) and lower in the oceanic zone (+2.7 days per decade for RCP8.5).

For beech, the increase in vegetation period compared to the historical period was equally driven by an earlier budburst and a later yellowing, except for the oceanic climate where the delay in leaf yellowing was more marked (Fig. A.1). For oak in continental and mountainous zones, the increase in vegetation period mainly originated from an earlier budburst while, in the oceanic zone, the earlier leafing and later yellowing were of similar magnitude (Fig. A.1).

3.2.2. Transpiration deficit

Transpiration deficit was strongly affected by the soil water reserve (MEW) and stand type and responded to the RCP scenarios in opposite ways for the two CO_2 modalities (Fig. 4). With $[CO_2]_{cst}$, transpiration deficit always significantly increased with the intensity of the radiative forcing. Whatever the RCP scenario used, soils with high soil water reserve (MEW) had a lower transpiration deficit than those with a low one. Under $[CO_2]_{var}$, transpiration deficit decreased with the radiative forcing intensity for the continental and oceanic climates while a slight increase was detected for the mountainous climate. Stands in the oceanic zone benefited the most from the decrease in transpiration deficit but still exhibited the highest level of transpiration deficit. The MEW effect was of the same magnitude for the $[CO_2]_{var}$ than for the $[CO_2]_{cst}$ modality. Stand type influenced transpiration deficit through a strong species composition effect (higher transpiration deficit for beech). However, the transpiration deficit response to climate change was not much affected by stand type (Fig. 4).

3.2.3. NPP

Compared to the historical period and assuming a $[CO_2]_{cst}$, median NPP slightly increased under continental and mountainous climates and remained more or less unchanged in the oceanic zone. The largest NPP increase occurred in the mountainous zone with high soil water reserve and amounted to 13.3% and 16.7% for RCP4.5 and RCP8.5, respectively (Fig. A.2). The RCP scenario effect on NPP was much more pronounced with the $[CO_2]_{var}$ runs (median NPP increase from 21.9% to 34.9% under RCP4.5 and from 35.7% to 63.1% under RCP8.5) but the modulation of this effect according to the soil water reserve (MEW) and the climate was less marked (Fig. A.2).

For the $[CO_2]_{cst}$ runs and the various virtual sites, the NPP changes between the historical period and 2071-2100 were comprised between –13.2% and +20.4% (median change: +7.30%) for RCP4.5 and between –28.8% and +27.8% (median change: +7.9%) for RCP8.5. Under the $[CO_2]_{var}$, the sites displayed NPP changes varying between +7.4% and +70.7% (median change: +30.7%) for RCP4.5 and between +7.6% and +126.6% (median change: +54.2%) for RCP8.5.

3.2.4. Comparison of the long-term trend with the inter-annual and inter-site variability and decomposition of the site effect

In order to evaluate the relative importance of the climate change effect compared to the climate inter-annual and inter-site variations, a linear mixed model was built to decompose the various sources of NPP variability. For the $[CO_2]_{cst}$, the climate scenario effect only explained 4.7% of the NPP variability, while the effects of the inter-annual climate variations (residual variability) accounted for 19.9%. The total site effect explained 66.3% of the NPP variability and was decomposed into three components: 43.7% for the stand, 14.1% for the soil and 8.5% for the climate effect. Nine percent of the NPP variability was attributed to interactions between the site components and the climate change scenario effects. These interactions with the site were dominated by the climate component (explaining 6.3% out of the 9.0%) representing the effect of the historical climate on the NPP response to climate change while the stand and soil effects explained a similar fraction of the remaining 2.7% (Table 2a).

Under $[CO_2]_{var}$, the proportion of the NPP variability explained by the RCP scenario was considerably higher and amounted to 28.5%. The inter-annual climate variations explained a lower proportion of the total NPP

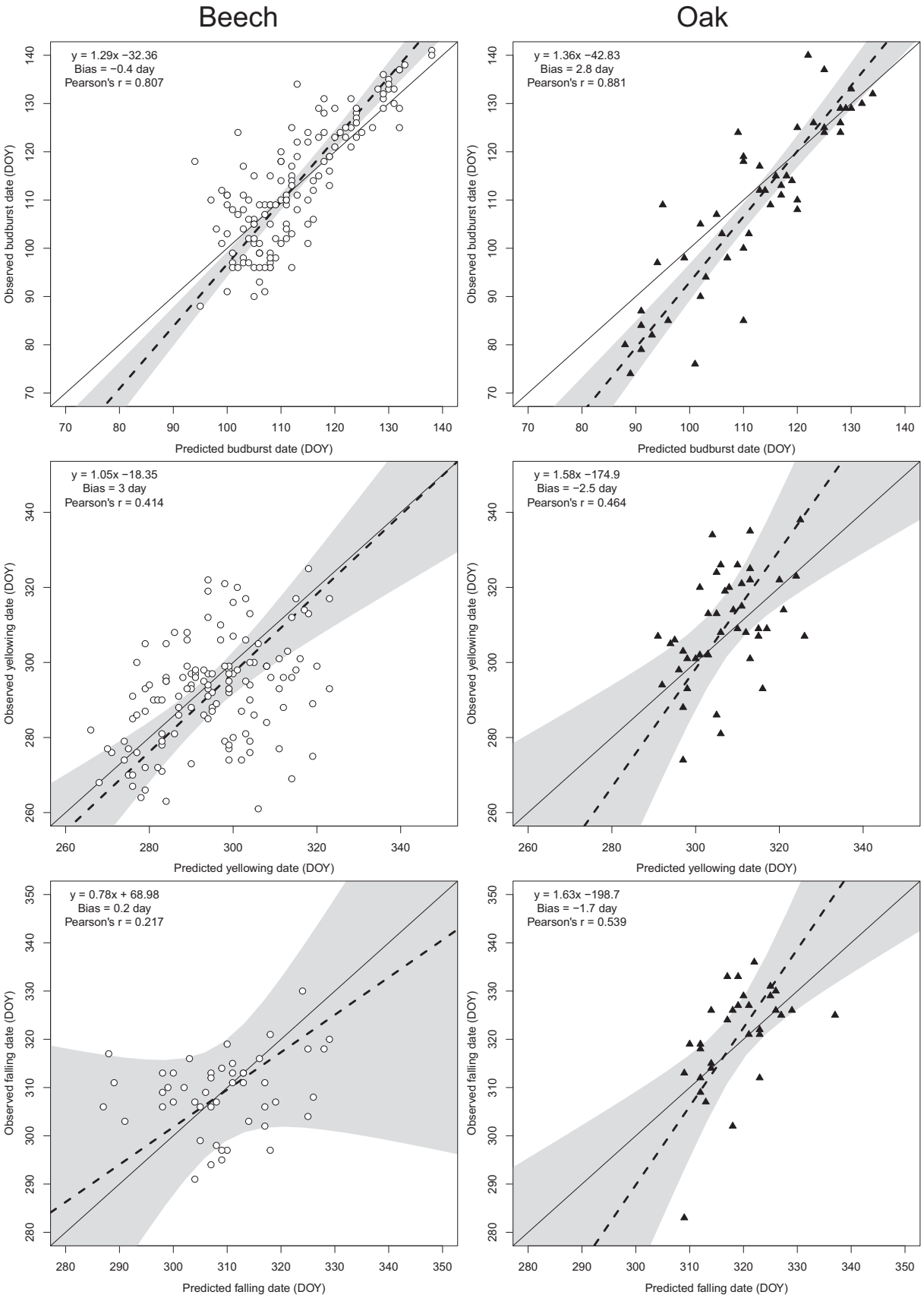

Fig. 2. Comparison of the observed and predicted mean stand budburst (top), yellowing (middle) and falling (bottom) dates for beech (left) and oak (right). The prediction quality is assessed based on the relative bias, the Pearson's r and the Deming regression test (position of the identity line (solid line) with respect to the confidence interval of the regression line (dashed line)).

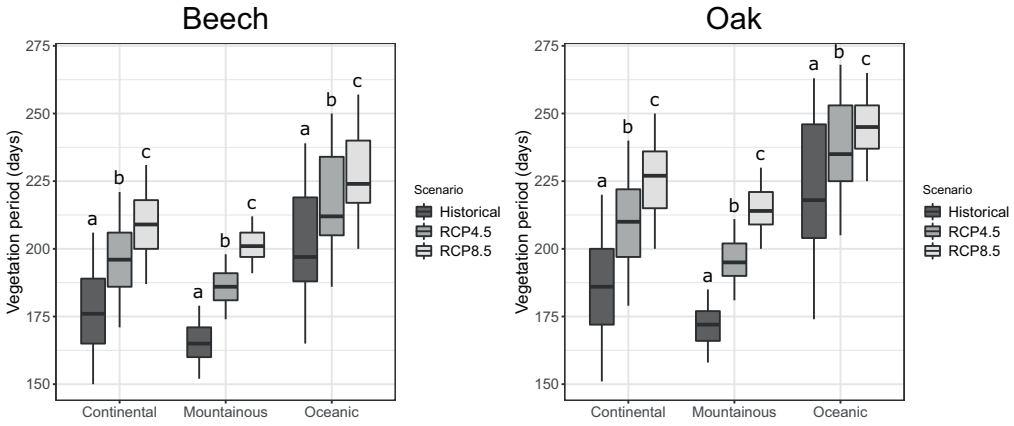

Fig. 3. Comparison of the vegetation period length in *virtual* sites simulated for the historical period (1976-2005) and for the future (2071-2100) according to two RCP scenarios; three climate types were considered as well as both tree species. For each box, the horizontal line corresponds to the median, the ends indicate the 25th and 75th percentiles and the whiskers show the values above and below these quartiles within 1.5 interquartile. For a same climate type, scenarios with common letters are not significantly different (paired Wilcoxon signed- rank between RCP4.5 and RCP8.5 and unpaired Mann-Whitney test between historical and RCP scenarios). The simulations made based on the two types of climate projections (CNRM-ALARO and IPSL-RCA4) were included in the analysis.

variability (16.4%). However, this NPP variability was higher than for the $[CO_2]_{cst}$ runs (+79.9%). Similarly, the site effect diminished but remained the major explaining factor with a partial R^2 of 0.476, which can be further divided in its stand (0.340), soil (0.069) and climate (0.067) components. Finally, the modulation of the climate scenario effect by the site components slightly decreased to explain 7.5% of the NPP variability with a dominance of the climate component (4.1%), followed by the stand (2.1%) and finally the soil (1.3%) (Table 2b).

To identify more precisely the factors at play behind the climate, soil and stand effects on NPP response to climate change, multivariate models were elaborated. For the $[CO_2]_{cst}$, the mean temperature during the vegetation period (for the historical period) was the main driver of the NPP change (17%), then the MAP change (10%) and the rainfall during the vegetation period for the historical period (5%). The beech proportion and the MEW both accounted for 2% of the variability in NPP change. Under $[CO_2]_{var}$, the mean temperature during the

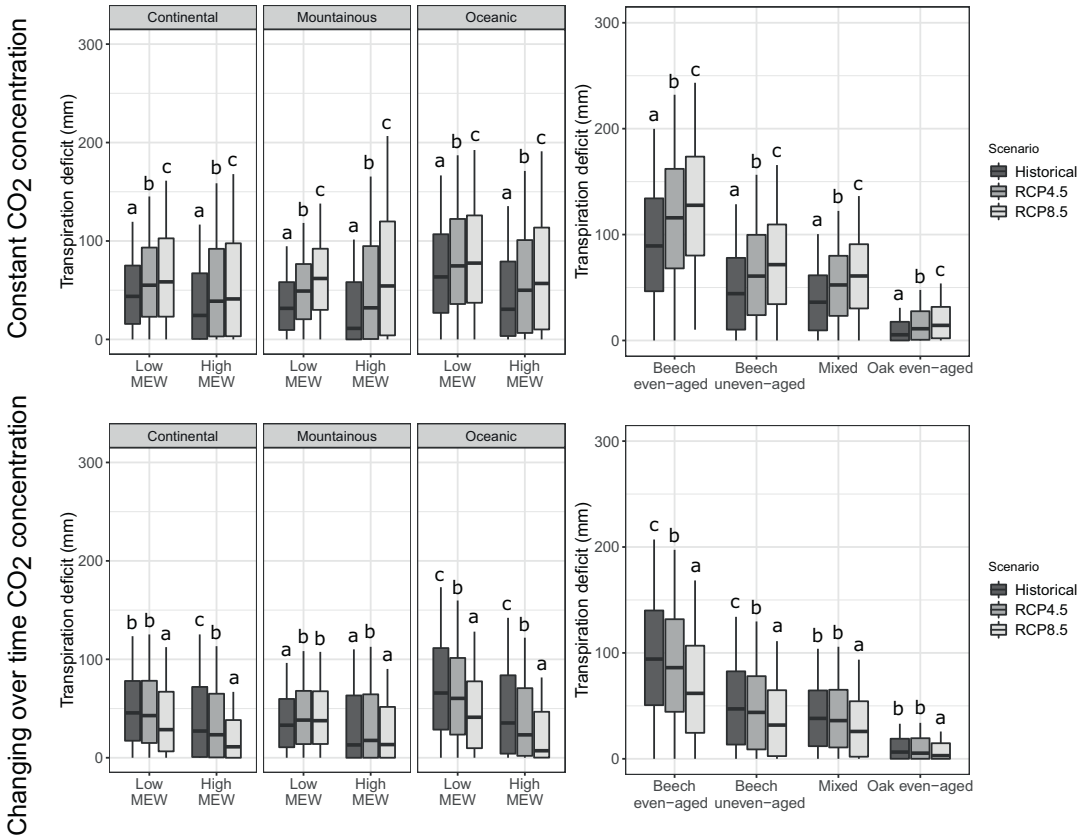

Fig. 4. Comparison of the simulated transpiration deficit in *virtual* sites among RCP scenarios (2071-2100) and the historical period (1976-2005) for the two atmospheric CO_2 modalities: highlighting of the climate zone, soil water reserve (MEW) and stand type effects. For each box, the horizontal line corresponds to the median, the ends indicate the 25th and 75th percentiles and the whiskers show the values above and below these quartiles within 1.5 interquartile. For a same stand, soil or climate type, scenarios with common letters are not significantly different (paired Wilcoxon signed- rank between RCP4.5 and RCP8.5 and unpaired Mann-Whitney test between historical and RCP scenarios). The simulations made based on the two types of climate projections (CNRM-ALARO and IPSL-RCA4) were included in the analysis.

Table 2
Estimate, standard error, P value and partial R^2 of the linear mixed model parameters (Eq. (3)) used to highlight the climate change effect and decompose the site effect in its climate, soil and stand components in order to explain the NPP ($gC\ m^{-2}\ yr^{-1}$) variability for the *virtual* sites with constant (a) and changing over time (b) atmospheric CO_2 concentration.

	Estimate	Standard error	*P* value	Partial R^2
a. Constant atmospheric CO_2 concentration				
Fixed effects				
Scenario [AL_Hist., AL_4.5, AL_8.5, RC_Hist, RC_4.5, RC_8.5]	[874.3, 956.9, 982.5, 836.7, 872.2, 851.5]	71.8	<0.0001	0.047
Random effects				
Stand	0	12,094.2	/	0.437
Soil	0	5855.5	/	0.141
Climate	0	3087.6	/	0.085
Stand × Scenario	0	165.8	/	0.013
Soil × Scenario	0	261.2	/	0.014
Climate × Scenario	0	917.7	/	0.063
Residuals	0	95.7	/	0.199
b. Changing over time atmospheric CO_2 concentration				
Fixed effects				
Scenario [AL_Hist., AL_4.5, AL_8.5, RC_Hist, RC_4.5, RC_8.5]	[848.2, 1094.2, 1286.6, 805.6, 1041.7, 1217.3]	79.1	<0.0001	0.285
Random effects				
Stand	0	16,443.3	/	0.340
Soil	0	5057.5	/	0.069
Climate	0	4143.3	/	0.067
Stand × Scenario	0	454.1	/	0.021
Soil × Scenario	0	425.7	/	0.013
Climate × Scenario	0	1033.2	/	0.041
Residuals	0	136.8	/	0.164

The scenario includes differences in climate projections due to both the RCP scenario (hist, 4.5 and 8.5) and to the climate models (CNRM-ALARO and IPSL-RCA4).

vegetation period was also the main driver (12%) but the stand variable played a more important role (mean dbh: 8% and basal area, BA,: 3.5%). All effects were positive except the mean temperature during the vegetation period (Table A.4). This effect was represented in Fig. 5. A significant decrease was observed with increasing temperature during vegetation period for all stand types and both CO_2 modalities but was more pronounced for the constant one. For the latter, the median change in NPP was negative in the mixed and even-aged oak stands with a mean temperature during the vegetation period (historical period) superior to 16 °C (Fig. 5).

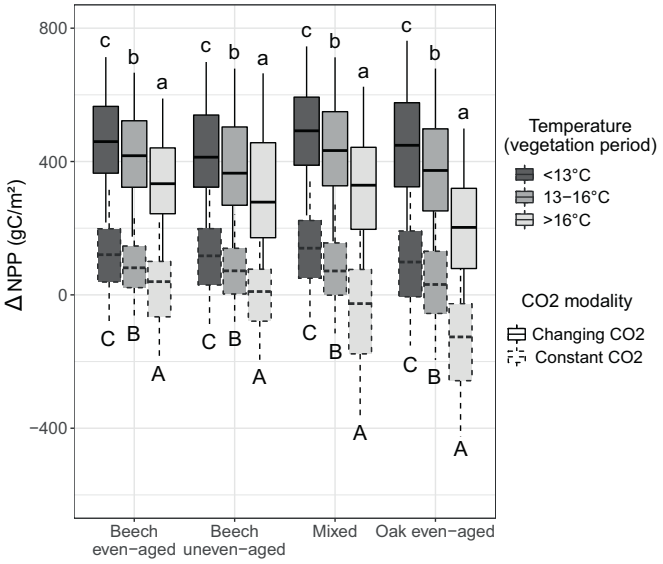

Fig. 5. Comparison of the simulated change in annual NPP in virtual sites between historical period (1976-2005) and RCP8.5 scenario (2071-2100) for the two atmospheric CO_2 modalities: highlighting of the stand type effect as well as the effects of the air temperature during the vegetation period. For each box, the horizontal line corresponds to the median, the ends indicate the 25th and 75th percentiles and the whiskers show the values above and below these quartiles within 1.5 interquartile. For a same stand type, temperatures during vegetation period with common letters are not significantly different (paired Wilcoxon signed- rank).

4. Discussion

4.1. Model calibration and performances

The model evaluation focused on individual tree height and radial growth over periods ranging mostly from 10 to 15 years. The predictions were better for the girth increment than for the tree height growth (Table 1). This difference in prediction capacity was already highlighted in other studies (e.g. Schwalm and Ek, 2004; Vospernik and Eckmüllner, 2012) and can be attributed, to some extent, to the measurement errors that are considerably higher for tree height than for girth, which affects model parameterisation, calibration and evaluation.

It is difficult to compare the evaluation results with other studies as the models applied on many sites across Europe are almost exclusively stand or cohort-based models, whose evaluation is done on observations averaged at the stand scale. Therefore, we compared our results to models that were locally and individually evaluated, which do not represent many studies as most individual-based models still make their evaluation at the stand-scale. Regarding girth increment, empirical models usually display the best results with relative biases most of the time below 13% and R^2 as high as 0.67 (Froese and Robinson, 2007; Mette et al., 2009; Schmid et al., 2006); while in process-based models, biases ranged between −30 and 30% and R^2 did not exceed 0.44 (Pretzsch, 2002; Thürig et al., 2005; Albrecht, 2007; Schmidt and Hansen, 2007; Kiernan et al., 2008). Based on the evaluation dataset, our prediction quality for girth increment was similar to that of empirical models for beech and intermediate between empirical and process-based models for oak. Tree height increment is much less evaluated and results differed considerably between the studies with relative biases covering a range from −70 to 61% and R^2 values from 0.04 to 0.48 (Sterba et al., 2001; Lacerte et al., 2006; Vospernik et al., 2007; Mette et al., 2009; Vospernik and Eckmüllner, 2012). With such a large span of statistical indices, our results easily fit in the range for bias but were at the lower margin regarding R^2.

4.2. Simulated climate change impacts

We chose to validate the model on a large panel of contrasting climates in order to improve its extrapolation ability to simulate the climate change impact in the future. In a certain way, we applied the space-for-time substitution but not with the classical approach, which considers that tree growth at a given location in a warmer future will follow the current tree growth in warmer locations. One of the limits of this space-for-time approach is that spatial variations in tree growth are not only due to climate but also to soil conditions, stand type and forest management (Gugger et al., 2010; Collalti et al., 2018; Klesse et al., 2019). In our study, we overcome these limits by validating a process-based model in space and use it for temporal extrapolation. The reinforcement of the approach lies in the description of the eco-physiological processes, which is more likely to remain valid for the future conditions than statistical relationships built on present-day climate.

We decided to simulate future tree growth for virtual sites created by combining various stands, soils and climates from existing sites in order to encompass the diversity of conditions in Europe. The reason for using virtual sites was to avoid correlations among the components of the site (soil, stand, climate) and to cover a large range of site

conditions and stand types while limiting the simulation number and the computing time.

4.2.1. Impact on vegetation period

Our predicted rates of change in budburst and yellowing dates for 2071-2100 are in agreement with other modelling studies. For beech, we found that budburst could advance between 0.5 and 2.1 days/decade and yellowing delay between 1.2 and 1.9 days/decade. This is consistent with values found in literature: 0.6 to 1.9 day/decade for budburst and 1.4 to 2.3 days/decade for yellowing (Davi et al., 2006; Menzel et al., 2008; Delpierre et al., 2009; Vitasse et al., 2011; Collalti et al., 2018; Zohner et al., 2020a). For oak, the 0.9 to 3.3 days/decade earlier budburst and the 0.8 to 1.4 days/decade later yellowing are also in agreement with the ranges found in the literature, knowingly 1.1 to 2.3 days/decade for budburst and 0.7 to 1.7 days/decade for yellowing (Davi et al., 2006; Menzel et al., 2008; Delpierre et al., 2009; Vitasse et al., 2011; Collalti et al., 2018; Nölte et al., 2020; Zohner et al., 2020a).

Interestingly, the greater advance in budburst for oak than for beech, compensated its initial delay during the historical period so that, in 2071-2100 under RCP8.5, budburst occurred more or less simultaneously for the two species (Fig. A.1). This stronger budburst sensitivity to temperature of oak compared to beech was highlighted in different studies (e.g. Vitasse et al., 2009; Cole and Sheldon, 2017). Regarding yellowing, the opposite trend was found, the greater delay in leaf senescence induced by climate warming for beech partly compensates for its earlier yellowing during historical period compared to oak. Finally, it is also interesting to note that, for oak, the photoperiod effect limited the yellowing delay induced by warmer temperature (Fig. A.1). These phenological changes and particularly budburst advances could be problematic as they increase the risk of late frost events during the tree leafing (Ma et al., 2019; Zohner et al., 2020b), for which oak and beech are particularly sensitive (San-Miguel-Ayanz et al., 2016; D'Andrea et al., 2020a; D'Andrea et al., 2020b).

4.2.2. Impact on water cycling

Under the assumption of $[CO_2]_{cst}$, a nearly generalized increase in transpiration deficit was observed. However, the level of transpiration deficit was strongly determined by the soil water reserve (MEW) and species composition. The soils with the highest MEW and the stands with the largest proportion of oak displayed the lowest deficits. These results agree with our expectations since sites with large soil water reserve are less subject to transpiration deficit and oaks are known to be less sensitive to drought than beech (Scherrer et al., 2011; Vanhellemont et al., 2019).

Two processes can increase the transpiration deficit: a higher evapotranspiration due to warmer air temperatures or the reduction in rainfall amount especially during the vegetation period. We observed that evapotranspiration increased on average by 17.1 and 25.1% for oak-dominated stands and by 10.4 and 16.8% for beech dominated stands for the scenarios RCP4.5 and RCP8.5, respectively while the rainfall during the vegetation period was reduced on average by 4.8 and 5.7%. However, a considerable influence of the climate model lies behind these values. In CNRM-ALARO, the evapotranspiration increase is 102% higher than with IPSL-RCA4. In the CNRM-ALARO projections under RCP4.5 and RCP8.5, the rainfall during the vegetation period increased by 4.0 and 8.2% while vegetation period rainfall decreases by 13.5 and 19.6% in IPSL-RCA4 projections. Such differences between climate models are known (Kjellström et al., 2018) and can mainly be ascribed to the GCM regarding summer rainfall (Christensen and Kjellström, 2020). In our case, the GCM CNRM-CM5 displays winter rainfall changes in line with most climate projections but for the summer they tend to be at the high end compared to the other CMIP5 models while IPSL-CMA5 presents rainfall changes in the middle of the range of the other models for all seasons (McSweeney et al., 2015). In addition, the RCM ALARO-0 associated to CNRM-CM5 also shows a tendency to produce wet summers as shown in Termonia et al. (2018). The two models considered here can be seen as illustrative of the sensitivity of our results to the uncertainty in the climate input. In the future, the use of climate projections from other GCM-RCM combinations would be interesting to better account for the large uncertainty linked to the climate modelling of precipitation changes (Goberville et al., 2015; Dyderski et al., 2018; Nölte et al., 2020).

Under the $[CO_2]_{var}$ modality and RCP8.5 scenario, the transpiration deficit decreased in continental and oceanic zones and for all stand types (Fig. 4). This confirms that, under higher CO_2 levels, the stomatal conductance regulation allowed increasing photosynthesis and CO_2 fixation while limiting water loss.

4.2.3. Impact on NPP

While NPP slightly increased for the $[CO_2]_{cst}$ runs in continental and mountainous climates and remained unchanged in the oceanic zone under the RCP8.5 scenario, NPP gains were observed everywhere and with greater magnitude with the $[CO_2]_{var}$ runs (Fig. A.2). Furthermore, NPP changes obtained with the $[CO_2]_{cst}$ runs were much more limited than those derived from the $[CO_2]_{var}$ runs (Fig. 5). The contrasting response of tree growth between the two CO_2 modalities can be ascribed to the enhanced photosynthesis and the lower stomatal conductance under elevated atmospheric CO_2 concentration, which induces higher water use efficiency (Ainsworth and Rogers, 2007; Norby and Zak, 2011). By comparing the two CO_2 modalities, we noticed that 60% to 100% of the NPP increase under $[CO_2]_{var}$ can be ascribed to the so called CO_2 fertilisation effect (Fig. 5). In other modelling studies comparing simulations with a constant and changing CO_2 modality for oak and beech, the contribution of the CO_2 fertilisation effect to the predicted productivity gain was pretty similar and amounted to 75% - 100% (Davi et al., 2006; Reyer et al., 2014; Collalti et al., 2018; Nölte et al., 2020).

This fertilisation effect was highlighted in Free-Air Carbon dioxide Enrichment (FACE) experiments (Ainsworth and Long, 2005; Norby et al., 2005). However, its persistence in time remains quite uncertain. It will depend on the way the nutrient demand and the uptake capacity of the trees will evolve as well as on the soil ability to satisfy the increased nutrient demand (Oren et al., 2001; Wieder et al., 2015). Indeed, as the water use efficiency is expected to increase with rising CO_2 concentration, nutrient use efficiency could also increase and allow maintaining productivity gain with a limited increase in nutrient demand (Caldararu et al., 2020). However, even if an increase in nutrient use efficiency could temporarily delay the appearance of nutritional limitations, the nutrient availability will constrain the productivity gains sooner or later and the stands installed on nutrient-poor soils will be potentially the first affected (Norby et al., 2010; Warren et al., 2015). A decline of the CO_2 fertilisation effect is already observed at the global scale (Terrer et al., 2019; Wang et al., 2020). Consequently, the most likely scenario lies probably in between the two CO_2 modalities and will be closer to one or the other depending on the nutrient availability of the site, which is not considered here. Except in nitrogen-saturated forest ecosystems, high nitrogen (N) deposition could help maintain a persistent CO_2 fertilisation effect (Etzold et al., 2020). With this regard, the current decline in N deposition in Europe will probably contribute to limit the increase in forest productivity (Waldner et al., 2015; Craine et al., 2018).

Under $[CO_2]_{cst}$ runs, the relative change in NPP (virtual sites and both RCP scenarios) amounted on average to +7% (−29 to 28%) while the changes reported in the literature for oak and beech in Europe are on average slightly negative (−2%) with decreases up to 15% and increases up to 10% (Albert et al., 2018; Collalti et al., 2018; Davi et al., 2006; Lasch et al., 2002; Nölte et al., 2020; Reyer et al., 2014; Sperlich et al., 2020). The slightly positive trend in NPP observed in our study is partly due to the overrepresentation of mountainous sites in which NPP more frequently increased than under the other climate zones (one third of our virtual sites were under mountainous climates) (Fig. A.2). The gain in NPP strongly decreased with the increase in temperature and turned into NPP decrease under the warmest climates for

mixed and even-aged oak stands (Fig. 5). Another reason explaining why our model simulated a positive median NPP change is linked to the climate projections we used, one of which predicting particularly high summer precipitations compared to other climate models.

Under $[CO_2]_{cst}$ runs, the length of the vegetation period was the main driver of the NPP change as also mentioned by Keenan et al. (2014) and Park et al. (2016). As photosynthesis is a temperature-dependent process reaching an optimum for leaf temperature between 20 and 30 °C and then declines (Yamori et al., 2013), the rise in air temperature favours GPP but up to some extent and is especially marked in colder climates. Among the processes acting negatively on NPP, the higher transpiration deficit observed for beech stands under $[CO_2]_{cst}$ reduced the NPP. Maintenance respiration is also influenced by temperature. This effect is accounted for in the CUE function (see Eq. (1)) for oak but not for beech as it was not significant.

For the sites in which the fertilizing CO_2 effect is not constrained ($[CO_2]_{var}$ runs), the long-term trend could account for 29% of NPP variability which would be nearly twice the inter-annual climate variations (Table 2). In this case, the expected change corresponds to an increase in productivity, which is favourable to forest growth and vitality. In sites more constrained, for example by nutrient availability, as represented by the $[CO_2]_{cst}$ runs, the long-term trend would explain a limited part of the NPP variability compared to the inter-site and inter-annual climate variations (Table 2).

A large part of the NPP variability is explained by the site effect which is dominated by its stand component (Table 2). In a more limited extend, the site also influenced the NPP response to climate change but, in this case, with a dominance of its climate component (Table 2). Some stand characteristics influenced however the NPP change which, under $[CO_2]_{cst}$, was more positive in stands with a higher beech proportion and, under $[CO_2]_{var}$, in stands with higher density and mean tree size (Table A.4). The positive effect of beech on NPP change is due to the fact that its CUE was not decreased with increasing MAT contrary to oak. A negative MAT effect on beech CUE was not considered as it was not significant based on the available observations. If a MAT effect similar to that on oak CUE had been included for beech, the tendency could have been reverse since oak is less sensitive to drought. Under $[CO_2]_{var}$, the stand characteristics favouring NPP change probably partly reflect the stand ability to intercept more solar radiation (the density and the mean tree size) and then to benefit more from the CO_2 fertilisation effect. With other climate projections conducting, for example, to drier conditions during the vegetation period, the role played by the stand characteristics could change. The effects of the stand characteristics on NPP and on its response to climate change show that the forester has the possibility to act on the stand productivity and to prepare forests to possible adverse effects of climate change by reinforcing forest resilience.

Our results might sound optimistic, especially for beech for which drought-induced growth decline has been observed at the southern edge of their distribution area (Charru et al., 2010; Zimmermann et al., 2015; D'Andrea et al., 2020a, 2020b), raising concern about their persistence under warmer and drier conditions (Noce et al., 2017). However, other studies point out opposite results (Tegel et al., 2014) or emphasize the swift recovery ability of beech after drought episodes (Vanhellemont et al., 2019). At the European scale, a very slight crown defoliation increase of 2.4% and 2.2% in 20 years is observed for beech and oak in the level II plots of ICP Forests (Timmerman et al., 2020). In addition, a 5% increase in basal area increment was detected between 1980 and 2007 for European beech in France as well as a 4% increase for sessile oak and 3% decline for pedonculate oak (Charru et al., 2017). Forrester et al. (2021b) reconstructing past growth with 3-PG obtained similar changes (12% increase in stem biomass between 1960 and 2010) for European beech in Switzerland. These rates of change in tree growth are intermediate between those we obtained with constant and changing CO_2 runs.

Even if the future climate is on average more favourable for tree growth, extreme events could occur occasionally and trigger mortality. Currently, HETEROFOR does not account for vitality loss and mortality due to hydraulic failure, late frost, storms and biotic causes. We plan to describe the mortality by hydraulic failure and the damages due to late frost in the next versions of the model but accounting for pest attacks and diseases is less straightforward. More data and knowledge are required before all mortality causes can be adequately addressed in individual-based models (Hartmann et al., 2018).

5. Conclusion and future prospects

Our simulation results showed that the climate change could have a positive effect on forest productivity in most sites, except those displaying particularly warm spring and summer temperatures and a strong reduction in rainfall. There is however a large uncertainty on the magnitude of this effect depending on the model used for the climate projections, the RCP scenarios and on whether the CO_2 fertilisation effect will persist or not. Apart from the CO_2 fertilisation, the main drivers of the positive changes are the increase in the vegetation period length and the improved water use efficiency. The negative NPP changes observed in some sites can be explained by higher transpiration deficit and maintenance respiration costs. While the site effect and mainly the stand characteristics explained the major part of the NPP variability, they showed only a limited influence on the forest response to climate change.

Given the strong influence of the choice of the climate model on our results, it would be interesting to repeat the simulations with climate projections from other models to still better apprehend the uncertainty associated with this aspect. With some climate projections, water stress could be more pronounced, especially in beech stands and lead to productivity losses in more sites.

CRediT authorship contribution statement

Louis de Wergifosse: Conceptualization, Formal analysis, Methodology, Software, Writing – original draft. **Frédéric Andre:** Software, Data curation, Writing – review & editing. **Hugues Goosse:** Supervision, Writing – review & editing. **Andrzej Boczon:** Resources, Writing – review & editing. **Sébastien Cecchini:** Resources, Writing – review & editing. **Albert Ciceu:** Resources, Writing – review & editing. **Alessio Collalti:** Resources, Writing – review & editing. **Nathalie Cools:** Resources, Writing – review & editing. **Ettore D'Andrea:** Resources, Writing – review & editing. **Bruno de Vos:** Resources, Writing – review & editing. **Rafiq Hamdi:** Resources, Writing – review & editing. **Morten Ingerslev:** Resources, Writing – review & editing. **Morten Alban Knudsen:** Resources, Writing – review & editing. **Anna Kowalska:** Resources, Writing – review & editing. **Stefan Leca:** Resources, Writing – review & editing. **Giorgio Matteucci:** Resources, Writing – review & editing. **Thomas Nord-Larsen:** Resources, Writing – review & editing. **Tanja GM Sanders:** Resources, Writing – review & editing. **Andreas Schmitz:** Resources, Writing – review & editing. **Piet Termonia:** Resources, Writing – review & editing. **Elena Vanguelova:** Resources, Writing – review & editing. **Bert V.A.N. Schaeybroeck:** Resources, Writing – review & editing. **Arne Verstraeten:** Resources, Writing – review & editing. **Lars Vesterdal:** Resources, Writing – review & editing. **Mathieu Jonard:** Conceptualization, Software, Supervision, Writing – review & editing.

Declaration of competing interest

The authors declare that they have no conflict of interest.

Acknowledgements

We are grateful to the ICP Forests, RENECOFOR and LTER monitoring networks for the provision of inventory data and to the Royal

Meteorological Institute for the climate projections. This study was funded by FRIA (grant no. 1.E005.18).

Appendix A. Supplementary data

Supplementary data to this article can be found online at https://doi.org/10.1016/j.scitotenv.2021.150422.

References

Ainsworth, E.A., Long, S.P., 2005. What have we learned from 15 years of free-air CO2 enrichment (FACE)? A meta-analytic review of the responses of photosynthesis, canopy properties and plant production to rising CO2. New Phytol. 165 (2), 351–372.

Ainsworth, E.A., Rogers, A., 2007. The response of photosynthesis and stomatal conductance to rising [CO2]: mechanisms and environmental interactions. Plant Cell Environ. 30 (3), 258–270.

Albert, M., Nagel, R.V., Sutmöller, J., Schmidt, M., 2018. Quantifying the effect of persistent dryer climates on forest productivity and implications for forest planning: a case study in northern Germany. For. Ecosyst. 5 (1), 1–21.

Albrecht, A., 2007. In: Nagel, J. (Ed.), Evaluierung des Waldwachstumssimulators Silva 2.2 anhand langfristiger ertragskundlicher Versuchsflächen in Baden-Württemberg. Sektion Ertragskunde Jahrestagung.

Anchukaitis, K.J., Evans, M.N., Kaplan, A., Vaganov, E.A., Hughes, M.K., Grissino-Mayer, H.D., Cane, M.A., 2006. Forward modeling of regional scale tree-ring patterns in the southeastern United States and the recent influence of summer drought. Geophys. Res. Lett. 33 (4).

Anderegg, W.R., Konings, A.G., Trugman, A.T., Yu, K., Bowling, D.R., Gabbitas, R., Zenes, N., 2018. Hydraulic diversity of forests regulates ecosystem resilience during drought. Nature 561 (7724), 538.

André, F, de Wergifosse, L, de Coligny, F, Beudez, N, Ligot, G, Gauthray-Guyénet, V, Courbaud, B, Jonard, M, n.d.. Radiative transfer modeling in structurally-complex stands: towards a better understanding of parametrization. Ann. For. Sci.. In press.

André, F., Jonard, M., Ponette, Q., 2008. Influence of species and rain event characteristics on stemflow volume in a temperate mixed oak–beech stand. Hydrol. Process. 22 (22), 4455–4466.

Ball, J.T., Woodrow, I.E., Berry, J.A., 1987. A model predicting stomatal conductance and its contribution to the control of photosynthetis under different environmental conditions. In: Biggins, J. (Ed.), Progress in Photosynthesis Research. 4, pp. 221–224.

Bates, D., Mächler, M., Bolker, B., Walker, S., 2014. Fitting Linear Mixed-effects Models Using lme4.

Bedia, J., Baño-Medina, J., Legasa, M.N., Iturbide, M., Manzanas, R., Herrera, S., Casanueva, A., San-Martín, D., Cofiño, A.S., Gutiérrez, J.M., 2020. Statistical downscaling with the downscaleR package (v3. 1.0): contribution to the VALUE intercomparison experiment. Geosci. Model Dev. 13 (3), 1711–1735.

Briseño-Reyes, J., Corral-Rivas, J.J., Solis-Moreno, R., Padilla-Martínez, J.R., Vega-Nieva, D.J., López-Serrano, P.M., López-Sánchez, C.A., 2020. Individual tree diameter and height growth models for 30 tree species in mixed-species and uneven-aged forests of Mexico. Forests 11 (4), 429.

Caldararu, S., Thum, T., Yu, L., Zaehle, S., 2020. Whole-plant optimality predicts changes in leaf nitrogen under variable CO2 and nutrient availability. New Phytol. 225 (6), 2331–2346.

Canham, C.D., LePage, P.T., Coates, K.D., 2004. A neighborhood analysis of canopy tree competition: effects of shading versus crowding. Can. J. For. Res. 34 (4), 778–787.

Charru, M., Seynave, I., Morneau, F., Bontemps, J.-D., 2010. Recent changes in forest productivity: an analysis of national forest inventory data for common beech (Fagus sylvatica L.) in North-Eastern France. For. Ecol. Manag. 260, 864–874.

Charru, M., Seynave, I., Hervé, J.C., Bertrand, R., Bontemps, J.D., 2017. Recent growth changes in Western european forests are driven by climate warming and structured across tree species climatic habitats. Ann. For. Sci. 74 (2), 33.

Christensen, O.B., Kjellström, E., 2020. Partitioning uncertainty components of mean climate and climate change in a large ensemble of european regional climate model projections. Clim. Dyn. 54 (9), 4293–4308.

Cole, E.F., Sheldon, B.C., 2017. The shifting phenological landscape: within-and between-species variation in leaf emergence in a mixed-deciduous woodland. Ecol. Evol. 7 (4), 1135–1147.

Collalti, A., Prentice, I.C., 2019. Is NPP proportional to GPP? Waring's hypothesis 20 years on. Tree Physiol. 39 (8), 1473–1483.

Collalti, A., Marconi, S., Ibrom, A., Trotta, C., Anav, A., d'Andrea, E., Matteucci, G., Montagnani, L., Gielen, B., Mammarella, I., Grünwald, T., Knohl, A., Berninger, F., Zhao, Y., Valentini, R., Santini, M., 2016. Validation of 3D-CMCC Forest ecosystem model (v. 5.1) against eddy covariance data for 10 European forest sites. Geosci. Model Dev. 9 (2), 479–504.

Collalti, A., Trotta, C., Keenan, T.F., Ibrom, A., Bond-Lamberty, B., Grote, R., Vicca, S., Reyer, C.P.O., Migliavacca, M., Veroustraete, F., Anav, A., Campioli, M., Scoccimarro, E., Sigut, L., Grieco, E., Cescatti, A., Matteucci, G., 2018. Thinning can reduce losses in carbon use efficiency and carbon stocks in managed forests under warmer climate. J. Adv. Mod Earth Syst. 10 (10), 2427–2452.

Collalti, A., Tjoelker, M.G., Hoch, G., Mäkelä, A., Guidolotti, G., Heskel, M., Petit, G., Ryan, M.G., Battipaglia, G., Matteucci, G., Prentice, I.C., 2020. Plant respiration: controlled by photosynthesis or biomass? Glob. Chang. Biol. 26 (3), 1739–1753.

Coppola, E., Nogherotto, R., Ciarlò, J.M., Giorgi, F., van Meijgaard, E., Kadygrov, N., Wulfmeyer, V., 2020. Assessment of the European climate projections as simulated by the large EURO-CORDEX regional and global climate model ensemble. J. Geophys. Res. Atmos. 126 (4), e2019JD032356.

Courbaud, B., de Coligny, F., Cordonnier, T., 2003. Simulating radiation distribution in a heterogeneous Norway spruce forest on a slope. Agric. For. Meteorol. 116, 1–18.

Couvreur, V., Vanderborght, J., Javaux, M., 2012. A simple three-dimensional macroscopic root water uptake model based on the hydraulic architecture approach. Hydrol. Earth Syst. Sci. 16, 2957–2971.

Craine, J.M., Elmore, A.J., Wang, L., Aranibar, J., Bauters, M., Boeckx, P., Zmudczyńska-Skarbek, K., 2018. Isotopic evidence for oligotrophication of terrestrial ecosystems. Nature Ecol. Evol. 2 (11), 1735–1744.

D'Andrea, E., Scartazza, A., Battistelli, A., Collalti, A., Proietti, S., Rezaie, N., Matteucci, G., Moscatello, S., 2020a. Unravelling resilience mechanisms in forests: role of non-structural carbohydrates in responding to extreme weather events. Tree Physiol. https://doi.org/10.1093/treephys/tpab044.

D'Andrea, E., Rezaie, N., Prislan, P., Gričar, J., Collalti, A., Muhr, J., Matteucci, G., 2020b. Frost and drought: effects of extreme weather events on stem carbon dynamics in a Mediterranean beech forest. Plant Cell Environ. 43 (10), 2365–2379.

Davi, H., Dufrêne, E., Francois, C., Le Maire, G., Loustau, D., Bosc, A., Sambal, S., Granier, A., Moors, E., 2006. Sensitivity of water and carbon fluxes to climate changes from 1960 to 2100 in european forest ecosystems. Agric. For. Meteorol. 141 (1), 35–56.

de Wergifosse, L., 2021. Simulating Tree Growth Response to Climate Change in Structurally-complex Oak and Beech Stands Across Europe. UCLouvain, Louvain-la-Neuve.

de Wergifosse, L., André, F., Beudez, N., de Coligny, F., Goosse, H., Jonard, F., Ponette, Q., Titeux, H., Vincke, C., Jonard, M., 2020a. HETEROFOR 1.0: a spatially explicit model for exploring the response of structurally complex forests to uncertain future conditions. II. Phenology and water cycle. Geosci. Model Dev. 13, 1459–1498.

de Wergifosse, L., André, F., Goosse, H., Caluwaerts, S., de Cruz, L., de Troch, R., van Schaeybroeck, B., Jonard, M., 2020b. CO2 fertilization, transpiration deficit and vegetation period drive the response of mixed broadleaved forests to a changing climate in Wallonia. Ann. For. Sci. 77 (3), 1–23.

Delpierre, N., Dufrêne, E., Soudani, K., Ulrich, E., Cecchini, S., Boé, J., François, C., 2009. Modelling interannual and spatial variability of leaf senescence for three deciduous tree species in France. Agric. For. Meteorol. 149 (6–7), 938–948.

Dufour-Kowalski, S., Courbaud, B., Dreyfus, P., Meredieu, C., De Coligny, F., 2012. Capsis: an open software framework and community for forest growth modelling. Ann. For. Sci. 69, 221–233.

Dufrêne, E., Davi, H., François, C., Le Maire, G., Le Dantec, V., Granier, A., 2005. Modelling carbon and water cycles in a beech forest: part I: model description and uncertainty analysis on modelled NEE. Ecol. Model. 185, 407–436.

Dufresne, J.L., Foujols, M.A., Denvil, S., Caubel, A., Marti, O., Aumont, O., Vuichard, N., 2013. Climate change projections using the IPSL-CM5 earth system model: from CMIP3 to CMIP5. Clim. Dyn. 40 (9), 2123–2165.

Dulamsuren, C., Hauck, M., Kopp, G., Ruff, M., Leuschner, C., 2017. European beech responds to climate change with growth decline at lower, and growth increase at higher elevations in the center of its distribution range (SW Germany). Trees 31 (2), 673–686.

Duputié, A., Rutschmann, A., Ronce, O., Chuine, I., 2015. Phenological plasticity will not help all species adapt to climate change. Glob. Chang. Biol. 21 (8), 3062–3073.

Dyderski, M.K., Paź, S., Frelich, L.E., Jagodziński, A.M., 2018. How much does climate change threaten European forest tree species distributions? Glob. Chang. Biol. 24 (3), 1150–1163.

Etzold, S., Ferretti, M., Reinds, G.J., Solberg, S., Gessler, A., Waldner, P., Schaub, M., Simpson, D., Benham, S., Hansen, K., Ingerslev, M., Jonard, M., Karlsson, P.E., Lindroos, A.J., Marchetto, A., Manninger, M., Meesenburg, H., Merilä, P., Nöjd, P., Rautio, P., Sanders, T.G.M., Seidling, W., Skudnik, M., Thimonier, A., Verstraeten, A., Vesterdal, L., Vejpustkova, M., de Vries, W., 2020. Nitrogen deposition is the most important environmental driver of growth of pure, even-aged and managed European forests. For. Ecol. Manag. 458, 117762.

FAO, 2012. Global Ecological Zones for FAO Forest Reporting: 2010 Update. Rome, Italy, FAO.

Ferretti, M., Fischer, R., 2013. Forest Monitoring: Methods for Terrestrial Investigations in Europe With an Overview of North America and Asia.

Forrester, D.I., Hobi, M.L., Mathys, A.S., Stadelmann, G., Trotsiuk, V., 2021a. Calibration of the process-based model 3-PG for major central European tree species. Eur. J. For. Res. 1–22.

Forrester, D.I., Mathys, A.S., Stadelmann, G., Trotsiuk, V., 2021b. Effects of climate on the growth of swiss uneven-aged forests: combining >100 years of observations with the 3-PG model. For. Ecol. Manag. 494, 119271.

Froese, R.E., Robinson, A.P., 2007. A validation and evaluation of the prognosis individual-tree basal area increment model. Can. J. For. Res. 37 (8), 1438–1449.

Giorgi, F., Jones, C., Asrar, G.R., 2009. Addressing climate information needs at the regional level: the CORDEX framework. World Meteorol. Org. Bull. 58 (3), 175.

Giot, O., Termonia, P., Degrauwe, D., De Troch, R., Caluwaerts, S., Smet, G., Berckmans, J., Deckmyn, A., De Cruz, L., De Meutter, P., Duerinckx, A., Gerard, L., Hamdi, R., Van den Bergh, J., Van Ginderachter, M., Van Schaeybroeck, B., 2016. Validation of the ALARO-0 model within the EURO-CORDEX framework. Geosci. Model Dev. 9 (3), 1143–1152.

Goberville, E., Beaugrand, G., Hautekèete, N.C., Piquot, Y., Luczak, C., 2015. Uncertainties in the projection of species distributions related to general circulation models. Ecol. Evol. 5 (5), 1100–1116.

Gugger, P.F., Sugita, S., Cavender-Bares, J., 2010. Phylogeography of Douglas-fir based on mitochondrial and chloroplast DNA sequences: testing hypotheses from the fossil record. Mol. Ecol. 19 (9), 1877–1897.

Hartmann, H., Moura, C.F., Anderegg, W.R., Ruehr, N.K., Salmon, Y., Allen, C.D., Arndt, S.K., Breshears, D.D., Davi, H., Galbraith, D., Ruthrof, K.X., Wunder, J., Adams, H.D.,

Bloemen, J., Cailleret, M., Cobb, R., Gessler, A., Grams, T., Jansen, S., Kautz, M., Lloret, F., O'Brien, M., 2018. Research frontiers for improving our understanding of drought-induced tree and forest mortality. New Phytol. 218 (1), 15–28.
Hersbach, H., Bell, B., Berrisford, P., Hirahara, S., Horányi, A., Muñoz-Sabater, J., Nicolas, J., Peubey, C., Radu, R., Schepers, D., Simmons, A., Soci, C., Abdalla, S., Abellan, X., Balsamo, G., Bechtold, P., Biavati, G., Bidlot, J., Bonavita, M., De Chiara, G., Dahlgren, P., Dee, D., Diamantakis, M., Dragani, R., Flemming, J., Forbes, R., Fuentes, M., Geer, A., Haimberger, L., Healy, S., Hogan, R.J., Hólm, E., Janisková, M., Keeley, S., Laloyaux, P., Lopez, P., Lupu, C., Radnoti, G., de Rosnay, P., Rozum, I., Vamborg, F., Villaume, S., Thépaut, J.-N., 2020. The ERA5 global reanalysis. Q. J. R. Meteorol. Soc. 146 (730), 1999–2049.
36 more authorsJacob, D., Petersen, J., Eggert, B., Alias, A., Christensen, O.B., Bouwer, L.M., Braun, A., Colette, A., Déqué, M., Georgievski, G., Georgopoulou, E., Gobiet, A., Menut, L., Nikulin, G., Haensler, A., Hempelmann, N., Jones, C., Keuler, K., Kovats, S., Kröner, N., Kotlarski, S., Kriegsmann, A., Martin, E., van Meijgaard, E., Moseley, C., Pfeifer, S., Preuschmann, S., Radermacher, C., Radtke, K., Rechid, D., Rounsevell, M., Samuelsson, P., Somot, S., Soussana, J.F., Teichmann, C., Valentini, R., Vautard, R., Weber, B., Yiou, P., 2014. EURO-CORDEX: new high-resolution climate change projections for European impact research. Reg. Environ. Change 14 (2), 563–578.
Jacob, D., Teichmann, C., Sobolowski, S., Katragkou, E., Anders, I., Belda, Wulfmeyer, V., Jacob, D., 2020. Regional climate downscaling over Europe: perspectives from the EURO-CORDEX community. Region. Env. Chang. (2), 1–20.
JMP®, Version 15. SAS Institute Inc., Cary, NC, 1989-2019.
Jonard, M., André, F., de Coligny, F., de Wergifosse, L., Beudez, N., Davi, H., Ligot, G., Ponette, Q., Vincke, C., 2020. HETEROFOR 1.0: a spatially explicit model for exploring the response of structurally complex forests to uncertain future conditions. I. Carbon fluxes and tree dimensional growth. Geosci. Model Dev. 13, 905–935.
Jucker, T., Bouriaud, O., Coomes, D.A., 2015. Crown plasticity enables trees to optimize canopy packing in mixed-species forests. Funct. Ecol. 29 (8), 1078–1086.
Jump, A.S., Hunt, J.M., Penuelas, J., 2006. Rapid climate change-related growth decline at the southern range edge of Fagus sylvatica. Glob. Change Biol. 12 (11), 2163–2174.
Keenan, T.F., Gray, J., Friedl, M.A., Toomey, M., Bohrer, G., Hollinger, D.Y., Richardson, A.D., 2014. Net carbon uptake has increased through warming-induced changes in temperate forest phenology. Nat. Clim. Chang. 4 (7), 598–604.
Kiernan, D.H., Bevilacqua, E., Nyland, R., 2008. Individual tree diameter growth model for sugar maple trees in uneven-aged northern hardwood stands under selection system. For. Ecol. Manag. 256 (9), 1579–1586.
Kjellström, E., Nikulin, G., Strandberg, G., Christensen, O.B., Jacob, D., Keuler, K., Vautard, R., 2018. European climate change at global mean temperature increases of 1.5 and 2 C above pre-industrial conditions as simulated by the EURO-CORDEX regional climate models. Earth Syst. Dyn. 9 (2), 459–478.
Klesse, S., DeRose, R.J., Babst, F., Black, B.A., Anderegg, L.D., Axelson, J., Ettinger, A., Griesbauer, H., Guiterman, C.H., Harley, G., Harvey, J.E., Lo, Y.H., Lynch, A.M., O'Connor, C., Restaino, C., Sauchyn, D., Shaw, J.D., Smith, D.J., Wood, L., Villanueva-Díaz, J., Evans, M.E., 2019. Continental-scale tree-ring-based projection of Douglas-fir growth: testing the limits of space-for-time substitution. Glob. Change Biol. 26 (9), 5146–5163.
Koch, G.W., Sillett, S.C., Jennings, G.M., Davis, S.D., 2004. The limits to tree height. Nature 428 (6985), 851–854.
Kölling, C., 2007. Klimahüllen von 27 waldbaumarten. AFZ Wald 23, 1242–1244.
Lacerte, V., Laroque, G.R., Woods, M., Parton, W.J., Penner, M., 2006. Calibration of the forest vegetation simulator (FVS) model to the main forest species in Ontario, Canada. Ecol. Mod. 199, 336–349.
Lasch, P., Badeck, F.W., Lindner, M., Suckow, F., 2002. Sensitivity of simulated forest growth to changes in climate and atmospheric CO2. Forstwissenschaftliches Centralblatt 121, 155–171.
Ma, Q., Huang, J.G., Hänninen, H., Berninger, F., 2019. Divergent trends in the risk of spring frost damage to trees in Europe with recent warming. Glob. Chang. Biol. 25 (1), 351–360.
Maréchaux, I., Langerwish, F., Huth, A., Bugmann, H., Morin, X., Reyer, C.P.O., Seidl, R., Collalti, A., Dantas de Paula, M., Fischer, R., Gutsch, M., Lexer, M.J., Lischke, H., Rammig, A., Rödig, E., Sakschewski, B., Taubert, F., Thonicke, K., Vacchiano, G., Bohn, F.J., 2021. Tackling unresolved questions in forest ecology: The past and future role of simulation models. Ecol. Evol. 11 (9), 3746–3770. https://doi.org/10.1002/ece3.7391.
Martin-Benito, D., Pederson, N., 2015. Convergence in drought stress, but a divergence of climatic drivers across a latitudinal gradient in a temperate broadleaf forest. J. Biogeogr. 42 (5), 925–937.
McSweeney, C.F., Jones, R.G., Lee, R.W., Rowell, D.P., 2015. Selecting CMIP5 GCMs for downscaling over multiple regions. Clim. Dyn. 44 (11), 3237–3260.
Meinshausen, M., Smith, S.J., Calvin, K., Daniel, J.S., Kainuma, M.L., Lamarque, J.F., Montzka, S.A., Raper, S.C.B., Riahi, K., Thomson, A., Velders, G.J.M., Van Vuuren, D.P.P., 2011. The RCP greenhouse gas concentrations and their extensions from 1765 to 2300. Climat. Change 109 (1), 213–241.
Menzel, A., Estrella, N., Heitland, W., Susnik, A., Schleip, C., Dose, V., 2008. Bayesian analysis of the species-specific lengthening of the growing season in two european countries and the influence of an insect pest. Int. J. Biometeorol. 52 (3), 209–218.
Mette, T., Albrecht, A., Ammer, C., Biber, P., Kohnle, U., Pretzsch, H., 2009. Evaluation of the forest growth simulator SILVA on dominant trees in mature mixed silver fir–Norway spruce stands in South-West Germany. Ecol. Model. 220 (13–14), 1670–1680.
Monteith, J.L., 1965. Evaporation and environment. Symp. Soc. Exp. Biol. 19, 205–234.
Morin, X., Bugmann, H., de Coligny, F., Martin-StPaul, N., Cailleret, M., Limousin, J.M., Ourcival, J.M., Prevosto, B., Simioni, G., Toigo, M., Vennetier, M., Catteau, E., Guillemot, J., 2021. Beyond forest succession: a gap model to study ecosystem functioning and tree community composition under climate change. Funct. Ecol. 35 (4), 955–975.
Noce, S., Collalti, A., Santini, M., 2017. Likelihood of changes in forest species suitability, distribution, and diversity under future climate: the case of southern Europe. Ecol. Evol. 7 (22), 9358–9375.
Nölte, A., Yousefpour, R., Hanewinkel, M., 2020. Changes in sessile oak (Quercus petraea) productivity under climate change by improved leaf phenology in the 3-PG model. Ecol. Model. 438, 109285.
Norby, R.J., Zak, D.R., 2011. Ecological lessons from free-air CO2 enrichment (FACE) experiments. Annu. Rev. Ecol. Evol. Syst. 42.
Norby, R.J., DeLucia, E.H., Gielen, B., Calfapietra, C., Giardina, C.P., King, J.S., Ledford, J., McCarthy, H.R., Moore, D.J., Ceulemans, R., De Angelis, P., Finzi, A.C., Karnosky, D.F., Kubiske, M.E., Lukac, M., Pregitzer, K.S., Scarascia-Mugnozza, G.E., Schlesinger, W.H., Oren, R., 2005. Forest response to elevated CO2 is conserved across a broad range of productivity. PNAS 102 (50), 18052–18056.
Norby, R.J., Warren, J.M., Iversen, C.M., Medlyn, B.E., McMurtrie, R.E., 2010. CO2 enhancement of forest productivity constrained by limited nitrogen availability. PNAS 107 (45), 19368–19373.
Oren, R., Ellsworth, D.S., Johnsen, K.H., Phillips, N., Ewers, B.E., Maier, C., Schäfer, K., McCarthy, H., Hendrey, G., McNutty, S.G., Katul, G.G., 2001. Soil fertility limits carbon sequestration by forest ecosystems in a CO 2-enriched atmosphere. Nature 411 (6836), 469–472.
Park, T., Ganguly, S., Tømmervik, H., Euskirchen, E.S., Høgda, K.A., Karlsen, S.R., Myneni, R.B., 2016. Changes in growing season duration and productivity of northern vegetation inferred from long-term remote sensing data. Environ. Res. Lett. 11 (8), 084001.
Piao, S., Luyssaert, S., Ciais, P., Janssens, I.A., Chen, A., Cao, C., Fang, Y., Friedlingstein, P., Luo, Y., Wang, S., 2010. Forest annual carbon cost: a global-scale analysis of autotrophic respiration. Ecol. 91, 652–661.
Pretzsch, H., 2002. Application and evaluation of the growth simulator SILVA 2.2 for forest stands, forest estates and large regions. Forstwissenschaftliches Centralblatt 121, 28–51.
Pretzsch, H., Forrester, D.I., Rötzer, T., 2015. Representation of species mixing in forest growth models. A review and perspective. Ecol. Model. 313, 276–292.
R Core Team, 2020. R: A Language and Environment for Statistical Computing. R Foundation for Statistical Computing, Vienna, Austria.
Reyer, C., 2015. Forest productivity under environmental change—a review of stand-scale modelling studies. Curr. For. Rep. 1 (2), 53–68.
Reyer, C., Lasch-Born, P., Suckow, F., Gutsch, M., Murawski, A., Pilz, T., 2014. Projections of regional changes in forest net primary productivity for different tree species in Europe driven by climate change and carbon dioxide. Ann. For. Sci. 71 (2), 211–225.
Reyer, C.P., Silveyra Gonzalez, R., Dolos, K., Hartig, F., Hauf, Y., Noack, M., Lasch-Born, P., Rötzer, T., Pretzsch, H., Meesenburg, H., Fleck, S., Wagner, M., Bolte, A., Sanders, T.G.M., Kolari, P., Mäkelä, A., Vesala, T., Mammarella, I., Pumpanen, J., Collalti, A., Trotta, C., Matteucci, G., D'Andrea, E., Foltynova, L., Krejza, J., Ibrom, A., Pilegaard, K., Loustau, D., Bonnefond, J.M., Berbigier, P., Picart, D., Lafont, S., Dietze, M., Cameron, D., Vieno, M., Tian, H., Palacios-Orueta, A., Cicuendez, V., Recuero, L., Wiese, K., Büchner, M., Lange, S., Volkhoz, J., Kim, H., Horemans, J.A., Bohn, F., Steinkamp, J., Chikalanov, A., Weedon, G.P., Sheffield, J., Babst, F., Vega del Valle, I., Suckow, F., Martel, S., Mahnken, M., Gutsch, M., Frieler, K., 2020. The PROFOUND database for evaluating vegetation models and simulating climate impacts on european forests. ESSD 12 (2), 1295–1320.
Ruiz-Benito, P., Vacchiano, G., Lines, E.R., Reyer, C.P., Ratcliffe, S., Morin, X., Hartig, F., Mäkelä, A., Yousefpour, R., Chaves, J.E., Palacios-Orueta, A., Benito-Garzón, M., Morales-Molino, C., Camarero, J.J., Jump, A.S., Kattge, J., Lehtonen, A., Ibrom, A., Owen, H.J.F., Zavala, M.A., 2020. Available and missing data to model impact of climate change on European forests. Ecol. Model. 416, 108870.
Samuelsson, P., Jones, C.G., Ullerstig, A., Gollvik, S., ULF, Hansson, Wyser, K., Will' En, U., 2011. The Rossby Centre Regional Climate model RCA3: model description and performance. TELLUS A 63 (1), 4–23.
San-Miguel-Ayanz, J., de Rigo, D., Caudullo, G., Houston Durrant, T., Mauri, A. (Eds.), 2016. European Atlas of Forest Tree Species. Publ. Off. EU, Luxembourg.
Schäfer, K.V.R., Oren, R., Tenhunen, J.D., 2000. The effect of tree height on crown level stomatal conductance. Plant Cell Environ. 23, 365–375.
Scherrer, D., Bader, M.K.F., Körner, C., 2011. Drought-sensitivity ranking of deciduous tree species based on thermal imaging of forest canopies. Agric. For. Meteorol. 151 (12), 1632–1640.
Schmid, S., Zingg, A., Biber, P., Bugmann, H., 2006. Evaluation of the forest growth model SILVA along an elevational gradient in Switzerland. Eur. J. For. Res. 125 (1), 43–55.
Schmidt, M., Hansen, J., 2007. Validierung der Durchmesserzuwachsprognosen des Wachstumssimulators BWINPro 7.0 für Fichte und Buche für den Bereich der alten Bundesländer. In: Nagel, J. (Ed.), Sektion Ertragskunde Jahrestagung. Alsfeld-Eudorf, pp. 164–179.
Schwalm, C.R., Ek, A.R., 2004. A process-based model of forest ecosystems driven by meteorology. Ecol. Model. 179 (3), 317–348.
Sillmann, J., Kharin, V.V., Zwiers, F.W., Zhang, X., Bronaugh, D., 2013. Climate extremes indices in the CMIP5 multimodel ensemble: part 2. future climate projections. J. Geophys. Res. Atmos. 118 (6), 2473–2493.
Simioni, G., Marie, G., Huc, R., 2016. Influence of vegetation spatial structure on growth and water fluxes of a mixed forest: results from the NOTG 3D model. Ecol. Model. 328, 119–135.
Soil Science Division Staff, 2017. Soil survey manual. In: Ditzler, C., Scheffe, K., Monger, H.C. (Eds.), USDA Handbook 18. Government Printing Office, Washington, D.C.
Sperlich, D., Nadal-Sala, D., Gracia, C., Kreuzwieser, J., Hanewinkel, M., Yousefpour, R., 2020. Gains or losses in forest productivity under climate change? The uncertainty of CO2 fertilization and climate effects. Climate 8 (12), 141.
Spinoni, J., Barbosa, P., Bucchignani, E., Cassano, J., Cavazos, T., Christensen, J.H., Dosio, A., 2020. Future global meteorological drought hot spots: a study based on CORDEX data. J. Clim. 33 (9), 3635–3661.

Sterba, H., Korol, N., Rössler, G., 2001. Ein ansatz zur evaluierung eines einzelbaumwachstumssimulators für Fichtenreinbestände. Fw. Cbl. 120, 406–421.

Sykes, M.T., Prentice, I.C., Cramer, W., 1996. A bioclimatic model for the potential distributions of north European tree species under present and future climates. J. Biogeogr. 203–233.

Tegel, W., Seim, A., Hakelberg, D., Hoffmann, D., Panev, M., Westphal, T., Büntgen, U., 2014. A recent growth increase of European beech (Fagus sylvaticaL.) at its Mediterranean distribution limit contradicts drought stress. Eur. J. For. Res. 133, 61–71.

Termonia, P., Van Schaeybroeck, B., De Cruz, L., De Troch, R., Caluwaerts, S., Giot, O., Hamdi, R., Vannitsem, S., Duchêne, F., Willems, P., Tabari, H., Van Uytven, E., Hosseinzadehtalaei, P., Van Lipzig, N., Wouters, H., Vanden Broucke, S., van Ypersele, J.P., Marbaix, P., Villanueva-Birriel, C., Fettweis, X., Wyard, C., Scholzen, C., Doutreloup, S., De Ridder, K., Gobbin, A., Lauwaet, D., Stavrakou, T., Bauwens, M., Müller, J.F., Luyten, P., Ponsar, S., Van den Eynde, D., Pottiaux, E., 2018. The CORDEX. be initiative as a foundation for climate services in Belgium. Clim. Serv. 11, 49–61.

Terrer, C., Jackson, R.B., Prentice, I.C., Keenan, T.F., Kaiser, C., Vicca, S., Franklin, O., 2019. Nitrogen and phosphorus constrain the CO 2 fertilization of global plant biomass. Nat. Clim. Chang. 9 (9), 684–689.

Thürig, E., Kaufmann, E., Frisullo, R., Bugmann, H., 2005. Evaluation of the growth function of an empirical forest scenario model. For. Ecol. Manag. 204, 51–66.

Timmerman, V., Potocic, N., Ognjenovic, M., Kirchner, T., 2020. Tree crown conditions in 2019. Forest Condition in Europe: 2016 Technical Report of ICP Forests: Report Under the UNECE Convention on Long-range Transboundary Air Pollution (CLRTAP).

Tolwinski-Ward, S.E., Anchukaitis, K.J., Evans, M.N., 2013. Bayesian parameter estimation and interpretation for an intermediate model of tree-ring width. Clim. Past 9 (4), 1481–1493.

Trouvé, R., Bontemps, J.D., Seynave, I., Collet, C., Lebourgeois, F., 2015. Stand density, tree social status and water stress influence allocation in height and diameter growth of Quercus petraea (Liebl.). Tree Physiol. 35, 1035–1046.

Van Vuuren, D.P., Edmonds, J., Kainuma, M., Riahi, K., Thomson, A., Hibbard, K., Hurtt, G.C., Kram, T., Krey, V., Lamarque, J.F., Masui, T., Meinshausen, M., Nakicenovic, N., Smith, S.J., Rose, S.K., 2011. The representative concentration pathways: an overview. Clim. Chang. 109 (1), 5–31.

Vanhellemont, M., Sousa-Silva, R., Maes, S.L., Van den Bulcke, J., Hertzog, L., De Groote, S.R., Verheyen, K., 2019. Distinct growth responses to drought for oak and beech in temperate mixed forests. Sci. Total Environ. 650, 3017–3026.

Vitasse, Y., Porté, A.J., Kremer, A., Michalet, R., Delzon, S., 2009. Responses of canopy duration to temperature changes in four temperate tree species: relative contributions of spring and autumn leaf phenology. Oecologia 161 (1), 187–198.

Vitasse, Y., François, C., Delpierre, N., Dufrêne, E., Kremer, A., Chuine, I., Delzon, S., 2011. Assessing the effects of climate change on the phenology of european temperate trees. Agric. For. Meteorol. 151 (7), 969–980.

Voldoire, A., Sanchez-Gomez, E., Decharme, B., Cassou, C., Sénési, S., Valcke, S., Beau, I., Alias, A., Chevallier, M., Déqué, M., Deshayes, J., Douville, H., Fernandez, E., Madec, G., Maisonnave, E., Moine, M.P., Planton, S., Saint-Martin, D., Szopa, S., Tyteca, S., Alkama, R., Belamari, S., Braun, A., Coquart, L., Chauvin, F., Salas y Mélia, D., 2013. The CNRM-CM5. 1 global climate model: description and basic evaluation. Climat. Dyn. 40 (9), 2091–2121.

Vospernik, S., Eckmüllner, O., 2012. Evaluation of the individual tree growth model prognaus. Austrian J. For. Sci. 129, 22–55.

Vospernik, S., Bokalo, M., Reimoser, F., Sterba, H., 2007. Evaluation of a vegetation simulator for roe deer habitat predictions. Ecol. Mod. 202, 265–280.

Waldner, P., Thimonier, A., Pannatier, E.G., Etzold, S., Schmitt, M., Marchetto, A., Minaya, M., 2015. Exceedance of critical loads and of critical limits impacts tree nutrition across Europe. Ann. For. Sci. 72 (7), 929–939.

Wang, E., Engel, T., 1998. Simulation of phenological development of wheat crops. Agric. Syst. 58 (1), 1–24.

Wang, S., Zhang, Y., Ju, W., Chen, J.M., Ciais, P., Cescatti, A., Peñuelas, J., 2020. Recent global decline of CO2 fertilization effects on vegetation photosynthesis. Science 370 (6522), 1295–1300.

Warren, J.M., Jensen, A.M., Medlyn, B.E., Norby, R.J., Tissue, D.T., 2015. Carbon dioxide stimulation of photosynthesis in Liquidambar styraciflua is not sustained during a 12-year field experiment. AoB Plants 7.

Wieder, W.R., Cleveland, C.C., Smith, W.K., Todd-Brown, K., 2015. Future productivity and carbon storage limited by terrestrial nutrient availability. Nature Geosci. 8 (6), 441–444.

Wilcoxon, F., 1945. Individual comparisons by ranking methods. Biom. Bull. 1 (6), 80–83.

Yamori, W., Hikosaka, K., Way, D.A., 2013. Temperature response of photosynthesis in C3, C4, and CAM plants: temperature acclimation and temperature adaptation. Photosynth. Res. 119, 101–117.

Zimmermann, J., Hauck, M., Dulamsuren, Ch., Leuschner, C., 2015. Climate warming-related growth decline affects Fagus sylvatica, but not other broad-leaved tree species in central european mixed forests. Ecosystems 18, 560–572.

Zohner, C.M., Mo, L., Pugh, T.A., Bastin, F.J., Crowther, T.W., 2020a. Interactive climate factors restrict future increases in spring productivity of temperate and boreal trees. Glob. Chang. Biol. 26 (7), 4042–4055.

Zohner, C.M., Mo, L., Renner, S.S., Svenning, J.C., Vitasse, Y., Benito, B.M., Crowther, T.W., 2020b. Late-spring frost risk between 1959 and 2017 decreased in North America but increased in Europe and Asia. PNAS 117 (22), 12192–12200.